Electronic Supplementary Material (ESI) for Chemical Communications.

The Number and Shape of Lattice Solvent Molecules Controls Spin-Crossover in an Isomorphous Series of Crystalline Solvate Salts

Izar Capel Berdiell[a,b], Rafal Kulmaczewski[a], Namrah Shahid[a], Oscar Cespedes[c] and Malcolm A. Halcrow[a,*]

[a]*School of Chemistry, University of Leeds, Woodhouse Lane, Leeds LS2 9JT, United Kingdom.*
E-mail: m.a.halcrow@leeds.ac.uk

[b]*Current address: Institute of Electronic Structure and Laser, Foundation for Research and Technology - Hellas, P.O. Box 1527, GR-711 10 Heraklion, Greece.*

[c]*School of Physics and Astronomy, University of Leeds, EC Stoner Building, Leeds LS2 9JT, United Kingdom.*

Supporting Information

Experimental

Synthesis

N-(2,6-di{pyrazol-1-yl}pyrid-4-yl)acetamide (*L*) was prepared by our previously reported procedure.[1]

CAUTION While we experienced no problems when using the perchlorate salts in this study, metal-organic perchlorates are potentially explosive and should be handled with care in small quantities.

Synthesis of [Fe*L*$_2$][BF$_4$]$_2$ (1[BF$_4$]$_2$) and [Fe*L*$_2$][ClO$_4$]$_2$ (1[ClO$_4$]$_2$). The various solvate crystals of these complex salts were obtained by combining the ligand and iron salt in different solvents. Separate solutions of *L* (25 mg, 0.093 mmol) and Fe[BF$_4$]$_2$·6H$_2$O (16 mg, 0.047 mmol) in the appropriate solvent (2x 5 cm^3) were mixed, causing an immediate intense yellow colouration. The resultant mixture was concentrated to 5 cm^3 volume, then crystallised by slow diffusion of diethyl ether vapour into the filtered solution to yield **1[BF$_4$]$_2$** as a yellow crystalline solid. Analogous procedures using Fe[ClO$_4$]$_2$·6H$_2$O (17 mg, 0.047 mmol) gave the corresponding solvates of **1[ClO$_4$]$_2$**. Crystallised yields range from 70-90 %.

Unless otherwise stated, the materials were dried *in vacuo* before being analysed. The alcohol solvates lost their lattice solvent upon drying at ambient temperature, yielding the solvent-free materials. The other crystalline solvates retain their solvent content with only **1[ClO$_4$]$_2$**·2MeNO$_2$ undergoing partial solvent loss on exposure to air according to the analytical formulations below.

The acetone solvates **1[BF$_4$]$_2$**·Me$_2$CO and **1[ClO$_4$]$_2$**·Me$_2$CO have been described elsewhere.[1]

For **1[BF$_4$]$_2$**: found C, 40.6; H, 3.19; N, 21.8 %. Calcd for $C_{26}H_{24}FeB_2F_8N_{12}O_2$: C, 40.8; H, 3.16; N, 21.9 %.

For **1[BF$_4$]$_2$**·2MeCN: found C, 42.4; H, 3.26; N, 22.9 %. Calcd for $C_{26}H_{24}FeB_2F_8N_{12}O_2{\cdot}2(CH_3CN)$ C, 42.5; H, 3.57; N, 23.1 %. This sample of **1[BF$_4$]$_2$**·*n*MeCN was simply air-dried before analysis.

For **1[BF$_4$]$_2$**·MeCN: found C, 41.7; H, 3.47; N, 22.6 %. Calcd for $C_{26}H_{24}FeB_2F_8N_{12}O_2{\cdot}CH_3CN$ C, 41.7; H, 3.37; N, 22.6 %. This sample of **1[BF$_4$]$_2$**·*n*MeCN was dried *in vacuo* for 24 hrs before being sent for analysis.

For **1[BF$_4$]$_2$**·EtCN: found C, 42.3; H, 3.41; N, 22.1 %. Calcd for $C_{26}H_{24}FeB_2F_8N_{12}O_2{\cdot}C_2H_5CN$ C, 42.4; H, 3.56; N, 22.2 %.

For **1[BF$_4$]$_2$**·2MeNO$_2$: found C, 37.6; H, 3.62; N, 22.2 %. Calcd for $C_{26}H_{24}FeB_2F_8N_{12}O_2{\cdot}2(CH_3NO_2)$ C, 37.9; H, 3.41; N, 22.1 %.

For **1[ClO$_4$]$_2$**: found C, 39.6; H, 3.13; N, 21.1 %. Calcd for $C_{26}H_{24}Cl_2FeN_{12}O_{10}$ C, 39.5; H, 3.06; N, 21.2 %.

For **1[ClO$_4$]$_2$**·CH$_3$CN: found C, 40.6; H, 3.11; N, 22.0 %. Calcd for $C_{26}H_{24}Cl_2FeN_{12}O_{10}{\cdot}CH_3CN$ C, 40.4; H, 3.27; N, 21.9 %.

For **1[ClO$_4$]$_2$**·EtCN: found C, 41.3; H, 3.30; N, 21.7 %. Calcd for $C_{26}H_{24}Cl_2FeN_{12}O_{10}{\cdot}C_2H_5CN$ C, 41.2; H, 3.45; N, 21.5 %.

For **1[ClO$_4$]$_2$**·MeNO$_2$: found C, 37.8; H, 3.23; N, 21.3 %. Calcd for $C_{26}H_{24}Cl_2FeN_{12}O_{10}{\cdot}CH_3NO_2$ C, 38.1; H, 3.19; N, 21.4 %. Single crystals of this compound have the formulation **1[ClO$_4$]$_2$**·2MeNO$_2$, so some lattice solvent was apparently lost from the sample in transit to the microanalysis lab.

Synthesis of [Fe*L*$_2$][BF$_4$]$_z$[ClO$_4$]$_{2-z}$ (1[BF$_4$]$_z$[ClO$_4$]$_{2-z}$; $z \approx 1$). Method as above, using equal quantities of Fe[BF$_4$]$_2$·6H$_2$O and Fe[ClO$_4$]$_2$·6H$_2$O (both 8 mg, 0.024 mmol) in methanol. Found C, 40.1; H, 3.26; N, 21.7 %. Calcd for $C_{26}H_{24}BClF_4FeN_{12}O_6$ C, 40.1; H, 3.11; N, 21.6 %.

Single Crystal Structure Analyses

All diffraction data were measured with an Agilent Supernova dual-source diffractometer using monochromated Cu-K_α (λ = 1.5418 Å) radiation. The diffractometer was fitted with an Oxford Cryostream low-temperature device. Experimental details of the structure determinations in this study are given in Tables S1-S2. All the structures were solved by direct methods *(SHELXS*[2]), and developed by full least-squares refinement on F^2 (*SHELXL-2018*[2]). Crystallographic figures were prepared using *XSEED*,[3] and octahedral coordination volumes (V_{Oh}) and Θ values were calculated with *Olex2*.[4]

Unless otherwise stated, all fully occupied non-H atoms in these refinements were refined anisotropically. Disordered anions were modelled with refined B–F/Cl–O and F···F/O···O distance restraints; and, disordered solvent was modelled using fixed bond length and angle restraints. All H atoms were placed in calculated positions and refined using a riding model.

Structure refinement of 1[BF_4]$_2$·2MeCN. All residues in the unit cell of this crystal lie on general crystallographic sites. One BF_4^- ion is disordered over two sites, with refined occupancies of 0.77:0.23. All non-H atoms except the disordered anion were refined anisotropically.

Structure refinement of 1[BF_4]$_2$·MeCN. Two datasets were measured from the same crystal, in its high-spin (200 K) and low-spin (125 K) state. The crystal is twinned at each temperature over two non-merohedral domains, which were resolved to afford reasonably precise refinements.

At 200 K the C atoms of one pyrazole ring in the complex cation were modelled as disordered over two half-occupied sites, to resolve an intermolecular steric clash between that group and its symmetry equivalent related by $-x$, $2-y$, $-z$. The fixed restraints C−C = 1.39(1), C−N = 1.36(1) and C=N = 1.32(1) Å were applied to that group. Both BF_4^- ions are disordered over two or three orientations, some of which share common B atoms. The acetonitrile molecule is also disordered over two sites, which were refined using fixed restraints C−C = 1.48(2), C−N = 1.15(2) and 1,3-C···N = 2.63(2) Å.

Structure refinements of 1[ClO_4]$_2$·MeCN. Two datasets were collected from the same crystal, at temperatures spanning its thermal spin transition. The structures were collected in order of decreasing temperature.

At 200 K the high-spin crystal included a minor (*ca* 25 %) non-merohedral twin domain, which was successfully resolved to allow a precise refinement. The C atoms of one pyrazole ring in the complex cation were modelled as disordered over two half-occupied sites, which was treated as for **1[BF_4]$_2$**·MeCN. Both ClO_4^- ions are disordered at these temperatures over three equally occupied sites; in one case, two of these sites share a common Cl atom. The acetonitrile molecule is also disordered over two sites, which were refined using fixed restraints C−C = 1.48(2), C−N = 1.15(2) and 1,3-C···N = 2.63(2) Å.

At 160 K the crystal has transformed to its low-spin state. One ClO_4^- ion is now crystallographically ordered, while the other anion is now disordered over two orientations. The solvent disorder is still present at this lower temperature, and was treated as above. The minor twinning noted in the high-spin datasets is not apparent at this temperature.

Structure refinements of 1[BF_4]$_2$·EtCN. Three datasets were collected from the same crystal, at temperatures spanning its thermal spin transition. The structures were collected in order of decreasing temperature. The crystal is twinned at each temperature over two approximately equally populated non-merohedral domains, which were successfully resolved at each temperature to allow precise refinements.

The asymmetric unit of the crystal contains one formula unit, with all residues occupying general crystallographic sites.

At 200 K (high-spin state), the C atoms of one pyrazole ring were modelled as disordered over two half-occupied sites, as described above for **1[BF_4]$_2$**·MeCN. One BF_4^- ion is disordered at these temperatures over two half-occupied sites. The propionitrile molecule is also disordered over two 0.5-occupied orientations, which were refined using fixed restraints CH_3−CH_2 = 1.51(2), CH_2−C(N) = 1.48(2), C−N = 1.15(2), 1,3-C···C = 2.44(2) and 1,3-C···N = 2.63(2) Å.

The refinement protocol at 187 K (mixed spin state) is the same is at 200 K, except for the pyrazolyl group which was modelled as crystallographically ordered. No disorder is present at 160 K, when the crystal is low-spin.

Structure refinements of 1[ClO_4]$_2$·EtCN. Three datasets were collected from the same crystal, at temperatures spanning its thermal spin transition. These structures were measured in order of increasing temperature. The crystal was twinned by a non-merohedral, 180° rotation about the unit cell *c* axis, which became more severe after the phase 1→2 transformation. These twin domains were successfully resolved in each dataset.

At 120 K the complex is low-spin, and all residues in the asymmetric unit are crystallographically ordered.

The structure at 170 K corresponds to a plateau in the $\chi_M T$ *vs* T curve of the compound. The crystal has transformed to an intermediate phase, with the same triclinic space group but a doubled unit cell volume. The asymmetric unit of this intermediate phase contains two formula units of the compound. The only disorder present involves one of the unique propionitrile molecules, which was modelled over two sites with a 0.83:0.17 occupancy ratio. This was treated with the fixed restraints $CH_3{-}CH_2$ = 1.51(2), $CH_2{-}C(N)$ = 1.48(2), C−N = 1.15(2), 1,3-C···C = 2.44(2) and 1,3-C···N = 2.63(2) Å.

At 240 K the crystal has become fully high-spin, and has returned to its original unit cell. Both ClO_4^- ions are disordered at this temperature over two or three occupied orientations, while the EtCN molecule was disordered over two equally occupied sites which were modelled using the above restraints.

Structure refinements of 1[BF_4]$_{0.9}$[ClO_4]$_{1.1}$·EtCN. This mixed-anion crystal is isomorphous with the corresponding pure BF_4^- and ClO_4^- solvate salts. Three datasets were collected in order of decreasing temperature. The first two structures were collected from the same crystal, but a different crystal had to be used for the low temperature dataset following a diffractometer fault. Unlike the other propionitrile solvates, neither crystal exhibited any twinning during the experiments.

In each refinement, each anion site was modelled with distinct partial BF_4^- and ClO_4^- sites, whose bond lengths and angles were restrained but whose occupancies were allowed to refine. The two crystals used (which came from the same crystallisation vial) had an identical anion stoichiometry, within experimental error of these refined occupancies.

The BF_4^- fraction of one anion site at 250 K is additionally disordered over two equally populated orientations. The propionitrile molecule is also disordered over two equally occupied sites. This was treated with the fixed restraints $CH_3{-}CH_2$ = 1.51(2), $CH_2{-}C(N)$ = 1.48(2), C−N = 1.15(2), 1,3-C···C = 2.44(2) and 1,3-C···N = 2.63(2) Å. There is a Fourier hole of −1.4 eÅ^{-3} close to a partial Cl atom in one of the mixed anion sites.

At 180 K the crystal had transformed to the same intermediate mixed-spin phase as found for [FeL_2][ClO_4]$_2$·EtCN. As in that other structure, one the two unique solvent molecules is slightly disordered over two orientations, which were modelled as above. No other disorder (apart from the mixed anion sites) is present.

The low spin crystal at 125 K has again transformed back to its original high-temperature phase. No disorder is present in this model, beyond the mixed anion sites mentioned above.

Structure refinements of 1[BF_4]$_2$·2MeNO$_2$ and 1[ClO_4]$_2$·2MeNO$_2$. The asymmetric units of these isomorphous crystals contain half a formula unit, with Fe(1) lying on the crystallographic C_2 axis ½, y, ¼. No disorder is present in either model.

Structure refinement of 1[BF_4]$_2$·MeOH. All residues in the unit cell of this crystal lie on general crystallographic sites. All C- and N-bound H atoms were placed in calculated positions and refined using a riding model. The methanol hydroxyl H atom was located in the Fourier map and allowed to refine with U_{iso} = 1.5x U_{eq}{O}.

Structure refinement of 1[ClO_4]$_2$·½EtOH. The asymmetric unit contains one complex cation and two ClO_4^- anions on general crystallographic sites, and half an ethanol molecule spanning the crystallographic inversion centre. One ClO_4^- ion is disordered over two equally occupied sites, which were modelled with refined restraints. This anion accepts a hydrogen bond from the solvent, and its disorder correlates with the orientation of that solvent about its inversion centre. All non-H atoms except the disordered anion O atoms were refined anisotropically.

CCDC 2078647−2078664 contain the supplementary crystallographic data for this paper (Tables S1 and S2). These data can be obtained free of charge from The Cambridge Crystallographic Data Centre via **www.ccdc.cam.ac.uk/data_request/cif**.

Other measurements

Elemental microanalyses were performed by the microanalytical service at the London Metropolitan University School of Human Sciences. X-ray powder diffraction patterns were measured at room temperature using a Bruker D2 Phaser diffractometer. Thermogravimetric analyses employed a TA Instruments TGA Q50 analyser with a temperature ramp of 10 K min^{-1} under a stream of nitrogen gas.

Solid state magnetic susceptibility measurements were performed on a Quantum Design MPMS-3 VSM magnetometer, with an applied field of 5000 G and a scan rate of 5 $Kmin^{-1}$. A diamagnetic correction for the sample was estimated from Pascal's constants;[5] a diamagnetic correction for the sample holder was also applied. If required, samples were protected against solvent loss during the measurement inside tightly sealed plastic capsules, containing an atmosphere saturated with a drop of diethyl ether. Magnetic measurements in solution were obtained by Evans method using a Bruker Avance500 spectrometer operating at 500.13 MHz.[6] A diamagnetic correction for the sample,[5] and a correction for the variation of the density of the solvent with temperature,[7] were applied to these data.

Table S1 Experimental data for the crystal structures in this work.

	1[BF$_4$]$_2$·2MeCN	**1[BF$_4$]$_2$**·MeCN		**1[BF$_4$]$_2$**·EtCN			**1[BF$_4$]$_2$**·2MeNO$_2$
molecular formula	$C_{30}H_{30}B_2F_8FeN_{14}O_2$	$C_{28}H_{27}B_2F_8FeN_{13}O_2$		$C_{29}H_{29}B_2F_8FeN_{13}O_2$			$C_{28}H_{30}B_2F_8FeN_{14}O_6$
M_r	848.15	807.09		821.12			888.13
crystal class	triclinic	triclinic		triclinic			orthorhombic
space group	$P\bar{1}$	$P\bar{1}$		$P\bar{1}$			*Pbcn*
a / Å	8.0593(3)	8.2279(3)	8.2204(5)	8.2454(3)	8.2464(3)	8.2658(5)	20.7377(3)
b / Å	12.7731(7)	12.5396(6)	12.3298(10)	12.6105(6)	12.5340(9)	12.3645(10)	8.8852(2)
c / Å	18.7851(16)	17.5742(11)	17.2739(14)	17.8210(9)	17.7464(9)	17.5585(11)	19.6895(3)
α / °	96.071(6)[c]	83.354(5)	82.969(7)	84.191(4)	83.832(5)	83.555(6)	–
β / °	102.319(5)[c]	79.986(4)	79.317(6)	80.215(4)	79.727(4)	79.079(5)	–
γ / °	101.556(4)[c]	80.831(4)	85.481(6)	81.291(4)	82.425(5)	84.390(6)	–
V / Å^3	1828.5(2)	1755.54(16)	1704.7(2)	1799.57(14)	1782.48(17)	1745.5(2)	3627.96(11)
Z	2	2	2	2	2	2	4
T / K	120(2)	200(2)	125(2)	200(2)	187(2)	160(2)	120(2)
μ{Cu-K_α} / mm^{-1}	4.136	4.268	4.395	4.173	4.213	4.303	4.283
D_c / gcm^{-3}	1.540	1.527	1.572	1.515	1.530	1.562	1.626
measured reflections	13810	6607[d]	6359[d]	11551[d]	11206[d]	10076[d]	8233
independent reflections	6908	6607[d]	6359[d]	11551[d]	11206[d]	10076[d]	3449
R_{int}	0.024	0[d]	0[d]	0[d]	0[d]	0[d]	0.022
parameters	515	514	491	488	491	500	269
restraints	22	64	0	38	30	0	1
R_1 [$F_0 > 4\sigma(F_0)$][a]	0.042	0.070	0.086	0.058	0.061	0.063	0.034
wR_2, all data[b]	0.111	0.211	0.252	0.165	0.172	0.175	0.088
goodness of fit	1.055	1.103	1.048	1.089	1.098	1.059	1.024
$\Delta\rho_{min/max}$ / eÅ^{-3}	–0.67/0.81	–0.56/0.75	–0.71/1.06	–0.55/0.72	–0.48/0.60	–0.49/0.57	–0.31/0.35
CCDC	2078647	2078648	2078649	2078652	2078653	2078654	2078661

[a] $R = \Sigma[\,|F_o| - |F_c|\,] / \Sigma|F_o|$ [b] $wR = [\Sigma w(F_o^2 - F_c^2) \;/\; \Sigma w F_o^4]^{1/2}$ [c] This unit cell is quoted with obtuse rather than acute angles, because it has opposite handedness when viewed down the shortest *a* axis (Figure S6). [d] This dataset was resolved into two non-merohedral twin domains. See pages S4-S5 for more details.

Table S1 continued.

	1[BF$_4$]$_2$·MeOH	**1[ClO$_4$]$_2$**·MeCN		**1[ClO$_4$]$_2$**·EtCN			**1[ClO$_4$]$_2$**·2MeNO$_2$
molecular formula	$C_{27}H_{28}B_2F_8FeN_{12}O_3$	$C_{28}H_{27}Cl_2FeN_{13}O_{10}$		$C_{29}H_{29}Cl_2FeN_{13}O_{10}$			$C_{28}H_{30}Cl_2FeN_{14}O_{14}$
M_r	798.08	832.38		846.40			913.41
crystal class	monoclinic	triclinic		triclinic			orthorhombic
space group	$P2_1/n$	$P\bar{1}$		$P\bar{1}$			$Pbcn$
a / Å	8.2085(2)	8.2794(3)	8.3202(8)	8.3297(4)	8.3390(2)	8.3394(3)	20.8034(15)
b / Å	38.9652(11)	12.6110(5)	12.3819(8)	12.6635(8)	20.3671(5)	12.3809(4)	8.8426(4)
c / Å	10.8625(3)	17.7349(8)	17.5192(9)	18.0861(10)	22.8144(7)	17.6807(5)	20.0469(15)
α / °	–	82.848(4)	81.925(5)	83.662(5)	108.029(3)[c]	82.191(3)	–
β / °	105.691(3)	79.767(3)	78.760(6)	80.003(4)	98.689(2)[c]	78.665(3)	–
γ / °	–	80.613(3)	85.352(6)	80.933(5)	95.458(2)[c]	85.142(3)	–
V / Å^3	3344.85(16)	1789.15(13)	1750.0(2)	1848.56(18)	3600.56(17)	1770.15(10)	3687.8(4)
Z	4	2	2	2	4	2	4
T / K	120(2)	200(2)	160(2)	240(2)	170(2)	120(2)	120(2)
μ\{Cu-K_α\} / mm^{-1}	4.485	5.400	5.521	5.236	5.376	5.464	5.390
D_c / gcm^{-3}	1.585	1.545	1.580	1.521	1.561	1.587	1.645
measured reflections	12628	6760[d]	13173	11656[d]	19048[d]	6668[d]	9763
independent reflections	6289	6760[d]	6578	11656[d]	19056[d]	6668[d]	3626
R_{int}	0.032	0[d]	0.046	0[d]	0[d]	0[d]	0.033
parameters	484	518	484	503	994	500	269
restraints	2	74	26	68	10	0	0
R_1 [$F_0 > 4\sigma(F_0)$][a]	0.062	0.059	0.088	0.076	0.075	0.058	0.038
wR_2, all data[b]	0.142	0.155	0.260	0.218	0.216	0.188	0.104
goodness of fit	1.143	1.066	1.098	1.100	1.039	1.101	1.030
$\Delta\rho_{min/max}$ / eÅ^{-3}	–0.43/0.51	–0.47/0.74	–0.81/0.97	–0.92/0.53	–0.58/0.75	–0.58/0.83	–0.38/0.31
CCDC	2078663	2078650	2078651	2078655	2078656	2078657	2078662

[a] $R = \Sigma[\,|F_o| - |F_c|\,] / \Sigma|F_o|$ [b] $wR = [\Sigma w(F_o^2 - F_c^2) \;/\; \Sigma wF_o^4]^{1/2}$ [c] This unit cell is quoted with obtuse rather than acute angles, because it has opposite handedness when viewed down the shortest a axis (Figure S6). [d] This dataset was resolved into two non-merohedral twin domains. See pages S4-S5 for more details.

Table S1 continued.

	1[ClO_4]$_2$·½EtOH	**1**[BF_4]$_{0.9}$[ClO_4]$_{1.1}$·EtCN		
molecular formula	$C_{27}H_{27}Cl_2FeN_{12}O_{10.5}$	$C_{29}H_{29}B_{0.9}Cl_{1.1}F_{3.6}FeN_{13}O_{6.4}$		
M_r	814.36	835.03		
crystal class	triclinic	triclinic		
space group	$P\bar{1}$	$P\bar{1}$		
a / Å	8.2123(7)	8.2960(2)	8.3062(3)	8.3093(4)
b / Å	10.9318(10)	12.6295(5)	20.4383(9)	12.3574(6)
c / Å	20.008(2)	18.0010(7)	22.6713(7)	17.5746(6)
α / °	79.143(9)	84.076(3)	108.026(3)[c]	82.690(3)
β / °	78.844(9)	80.160(3)	98.880(3)[c]	78.693(4)
γ / °	75.480(8)	81.045(3)	95.141(3)[c]	85.091(4)
V / Å^3	1687.4(3)	1829.95(11)	3577.1(2)	1751.76(13)
Z	2	2	2	2
T / K	120(2)	250(2)	180(2)	125(2)
μ{Cu-K_α} / mm^{-1}	5.712	4.756	4.866	4.968
D_c / gcm^{-3}	1.603	1.515	1.551	1.583
measured reflections	13392	14861	28990	13546
independent reflections	6407	6892	13444	6565
R_{int}	0.036	0.029	0.036	0.045
parameters	496	497	977	488
restraints	20	83	91	48
R_1 [$F_0 > 4\sigma(F_0)$][a]	0.047	0.073	0.068	0.050
wR_2, all data[b]	0.127	0.208	0.195	0.125
goodness of fit	1.029	1.089	1.052	1.029
$\Delta\rho_{min/max}$ / eÅ^{-3}	−0.46/0.73	−1.38/0.79	−1.19/0.88	−0.86/0.49
CCDC	2078664	2078658	2078659	2078660

[a]$R = \Sigma[\,|F_o| - |F_c|\,] / \Sigma|F_o|$ [b]$wR = [\Sigma w(F_o^2 - F_c^2) \;/\; \Sigma wF_o^4]^{1/2}$ [c]This unit cell is quoted with obtuse rather than acute angles, because it has opposite handedness when viewed down the shortest a axis (Figure S6). [d]This dataset was resolved into two non-merohedral twin domains. See pages S4-S5 for more details.

Definitions of the structural parameters in Tables S2, S6 and S11.

V_{Oh} is the volume (in Å^3) of the FeN_6 coordination octahedron in the complex,[8] which is typically <10 Å^3 in low-spin $[Fe(bpp)_2]^{2+}$ (bpp = 2,6-di{pyrazol-1-yl}pyridine) derivatives and ≥11.5 Å^3 in their high-spin form.[9]

Σ and Θ are defined as follows:

$$\Sigma = \sum_{i=1}^{12} |90 - \beta_i| \qquad \Theta = \sum_{j=1}^{24} |60 - \gamma_j|$$

where β_i are the twelve *cis*-N–Fe–N angles about the iron atom and γ_i are the 24 unique N–Fe–N angles measured on the projection of two triangular faces of the octahedron along their common pseudo-threefold axis (Scheme S1). Σ is a general measure of the deviation of a metal ion from an ideal octahedral geometry, while Θ more specifically indicates its distortion towards a trigonal prismatic structure. A perfectly octahedral complex gives $\Sigma = \Theta = 0$.[8,10]

Because the high-spin state of a complex has a much more plastic structure than the low-spin, this is reflected in Σ and Θ which are usually much larger in the high-spin state. The absolute values of these parameters depend on the metal/ligand combination in the compound under investigation, however. Typical values of these parameters for complexes related to $[FeL_2]^{2+}$ are given in refs. 11 and 12.

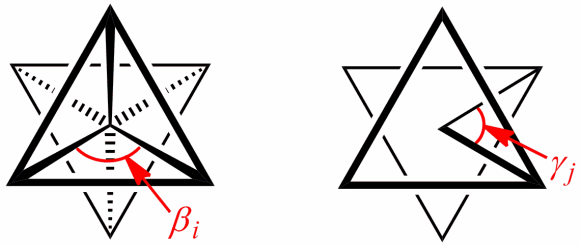

Scheme S1 Angles used in the definitions of the coordination distortion parameters Σ and Θ.

The parameters in Scheme S2 define the magnitude of an angular Jahn-Teller distortion, that is often observed in high-spin $[Fe(bpp)_2]^{2+}$ derivatives like $[FeL_2]^{2+}$ ($\theta \leq 90°$, $\phi \leq 180°$).[11-13] They are also a useful indicator of the molecular geometry, in defining the disposition of the two ligands around the metal ion. Spin-crossover can be inhibited if θ and ϕ deviate too strongly from their ideal values, because the associated rearrangement to a more regular low-spin coordination geometry ($\theta \approx 90°$, $\phi \approx 180°$) cannot be accommodated by a rigid solid lattice.[13-15] In less distorted examples, significant changes in θ and ϕ between the spin states can be associated with enhanced SCO cooperativity.[16]

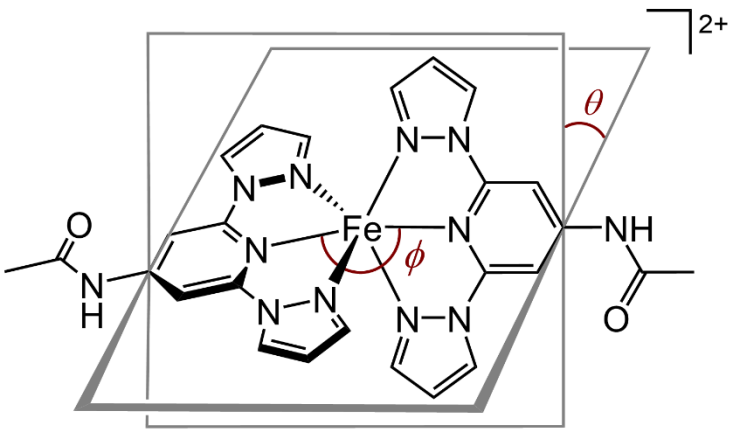

Scheme S2 θ and ϕ, used to discuss the structures of $[FeL_2]^{2+}$.

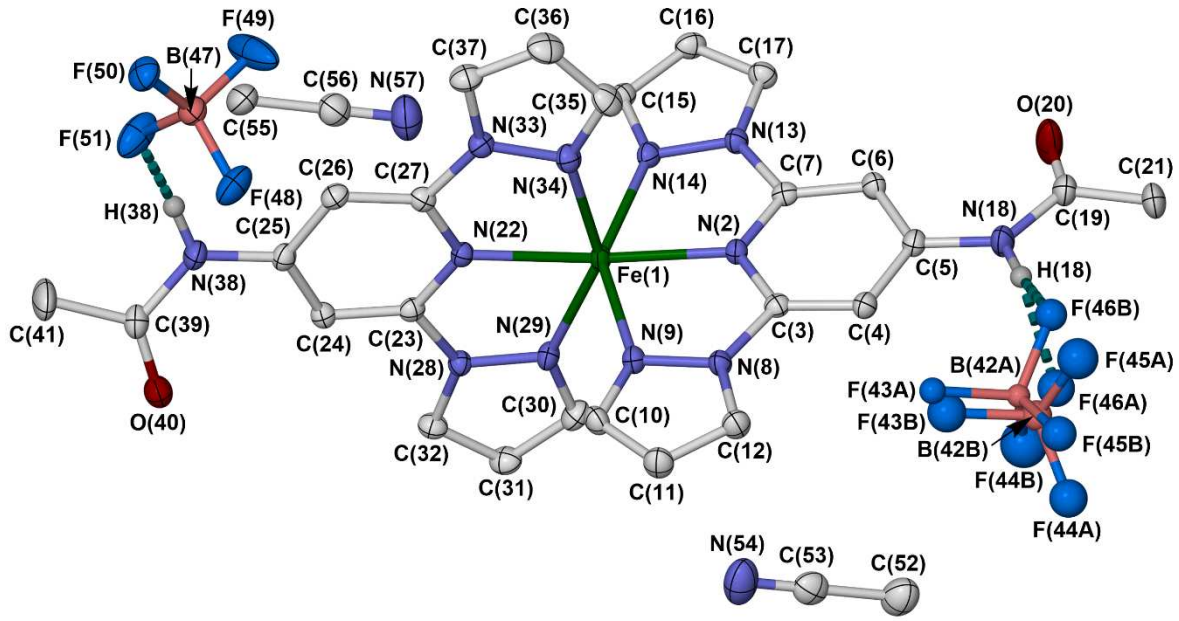

Figure S1 The asymmetric unit of **1[BF$_4$]$_2$**·2MeCN, with the full atom numbering scheme. Displacement ellipsoids are at the 50 % probability level, and C-bound H atoms are omitted for clarity.

Colour code: C, white; H, pale grey; B, pink; F, cyan; Fe, green; N, blue; O, red.

The main difference between this asymmetric unit and the isomorphous crystals **1X$_2$**·MeCN ($X^- = BF_4^-$ or ClO_4^-) is that solvent molecule C(55)-N(57) in this structure is missing in the mono-acetonitrile solvates (Figure S2).

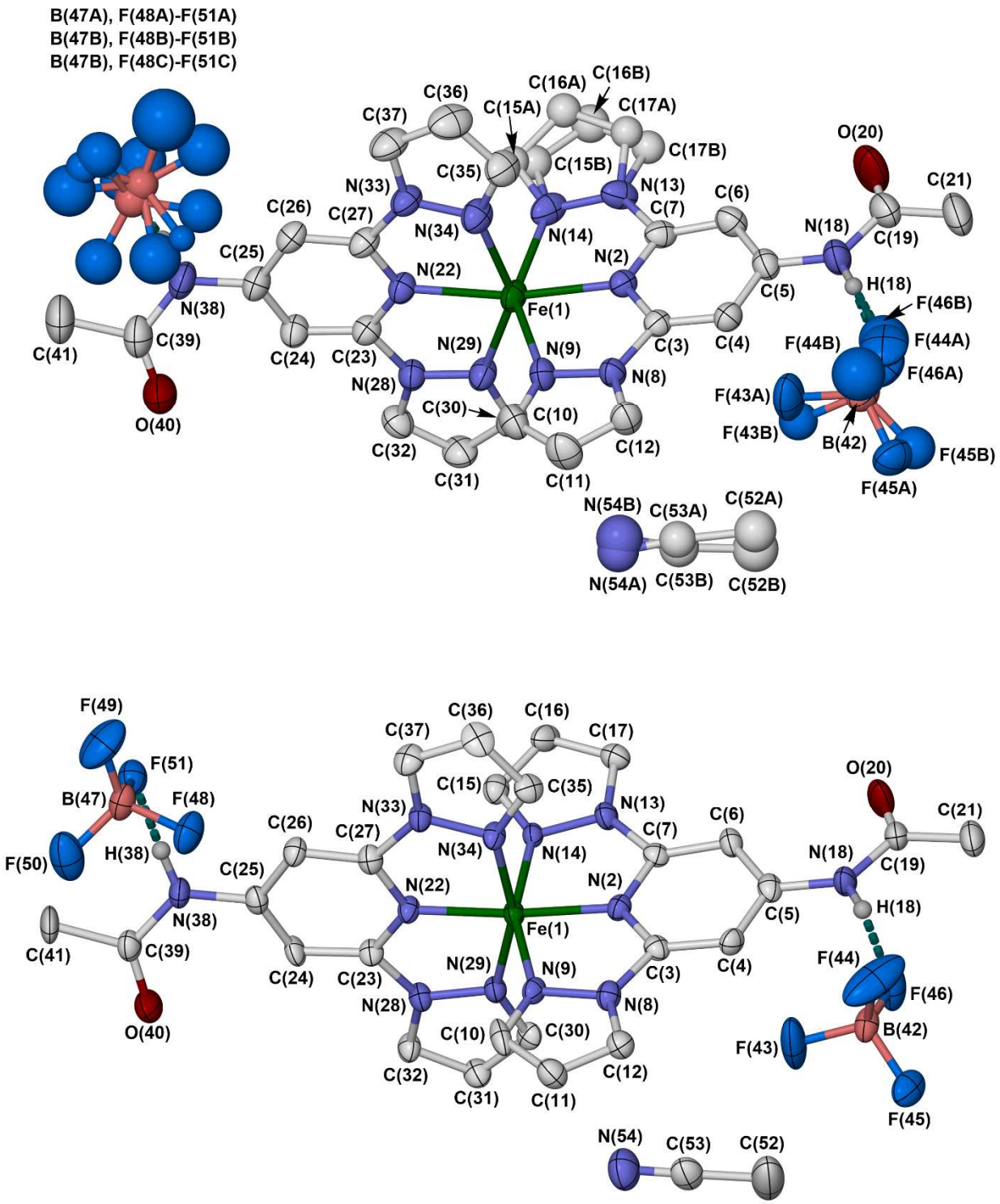

Figure S2 The asymmetric unit of **1[BF$_4$]$_2$**·MeCN at 200 K (top) and 125 K (bottom), with the full atom numbering scheme. Displacement ellipsoids are at the 50 % probability level, and C-bound H atoms are omitted.

Colour code: C, white; H, pale grey; B, pink; F, cyan; Fe, green; N, blue; O, red.

Atoms in the three-fold disordered anions in the higher temperature structure are not individually numbered, for clarity. The 'B' and 'C' orientations of anion B(47)-F(51) share a common partial B atom, B(47B).

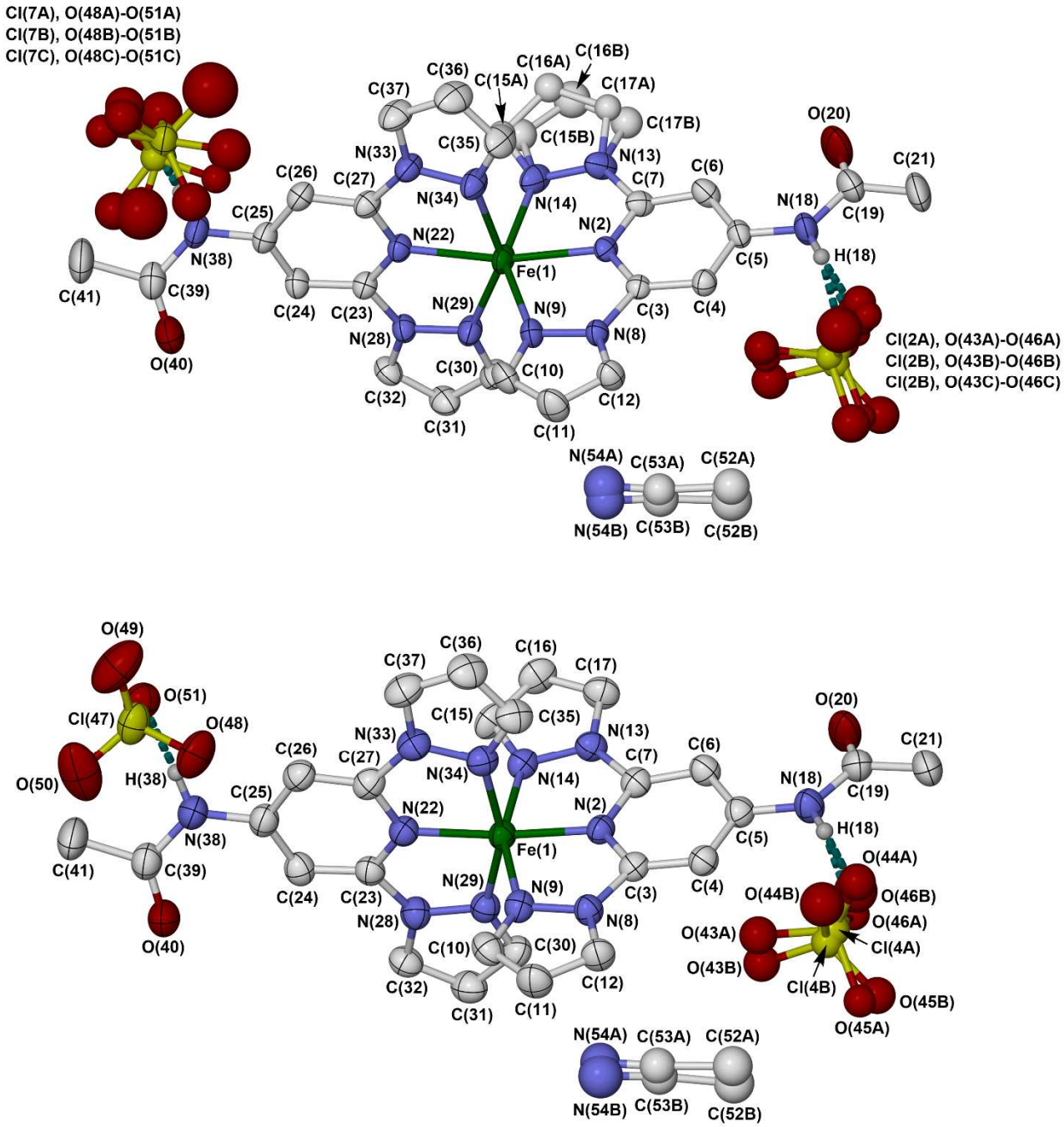

Figure S3 The asymmetric unit of **1[ClO$_4$]$_2$**·MeCN at 200 K (top) and 160 K (bottom), with the full atom numbering scheme. Displacement ellipsoids are at the 50 % probability level, and C-bound H atoms are omitted.

Colour code: C, white; H, pale grey; Cl, yellow; Fe, green; N, blue; O, red.

Atoms in the three-fold disordered anions in the higher temperature structure are not individually numbered, for clarity. The 'B' and 'C' orientations of anion Cl(42)-O(46) share a common partial Cl atom, Cl(2B).

Table S2 Selected bond lengths, angles and other structural parameters (Å , °, Å^3) for the acetonitrile solvates of **1X$_2$** (X^- = BF_4^- or ClO_4^-). See Figures S1-S3 for the atom numbering scheme, while definitions of V_{Oh}, Σ, Θ, φ and θ are given on page S10.

	1[BF$_4$]$_2$·2MeCN	**1[BF$_4$]$_2$**·MeCN		**1[ClO$_4$]$_2$**·MeCN	
T / K	120	200	125	200	160
Fe(1)–N(2)	2.1191(17)	2.111(3)	1.901(5)	2.119(3)	1.922(4)
Fe(1)–N(9)	2.2151(17)	2.195(4)	1.988(6)	2.193(3)	2.019(5)
Fe(1)–N(14)	2.2003(18)	2.178(4)	1.964(5)	2.176(3)	1.965(5)
Fe(1)–N(22)	2.1427(17)	2.125(3)	1.896(5)	2.132(3)	1.921(5)
Fe(1)–N(29)	2.1850(18)	2.180(4)	1.987(5)	2.185(3)	2.001(5)
Fe(1)–N(34)	2.2200(19)	2.196(4)	1.962(5)	2.200(3)	1.986(5)
N(2)–Fe(1)–N(9)	73.08(6)	73.34(13)	79.5(2)	73.19(11)	79.44(19)
N(2)–Fe(1)–N(14)	73.50(6)	73.65(14)	79.9(2)	73.47(11)	79.32(19)
N(2)–Fe(1)–N(22)	166.04(7)	168.66(14)	174.6(2)	167.79(11)	174.4(2)
N(2)–Fe(1)–N(29)	119.23(7)	117.18(14)	104.3(2)	117.76(11)	105.2(2)
N(2)–Fe(1)–N(34)	95.10(6)	96.89(14)	95.9(2)	96.23(11)	95.7(2)
N(9)–Fe(1)–N(14)	146.57(6)	146.96(14)	159.4(2)	146.65(11)	158.8(2)
N(9)–Fe(1)–N(22)	100.95(6)	111.34(14)	103.8(2)	112.89(11)	103.9(2)
N(9)–Fe(1)–N(29)	91.01(6)	95.14(14)	92.4(2)	94.93(12)	92.8(2)
N(9)–Fe(1)–N(34)	94.41(7)	94.85(15)	93.1(2)	95.46(12)	93.2(2)
N(14)–Fe(1)–N(22)	111.83(6)	100.89(14)	96.7(2)	99.76(12)	97.3(2)
N(14)–Fe(1)–N(29)	104.47(7)	100.98(15)	92.7(2)	101.06(12)	92.9(2)
N(14)–Fe(1)–N(34)	89.41(7)	87.74(16)	89.0(2)	87.44(13)	88.7(2)
N(22)–Fe(1)–N(29)	72.80(6)	73.30(14)	79.9(2)	73.11(11)	79.3(2)
N(22)–Fe(1)–N(34)	72.48(6)	72.71(14)	79.9(2)	73.03(11)	79.6(2)
N(29)–Fe(1)–N(34)	145.26(7)	145.92(14)	159.7(2)	146.01(12)	158.9(2)
V_{Oh}	12.415(7)	12.236(14)	9.543(16)	12.256(11)	9.803(15)
Σ	155.7(2)	155.9(4)	90.7(7)	157.3(6)	94.6(7)
Θ	511	502	292	505	303
ϕ	166.04(7)	168.66(14)	174.6(2)	167.79(11)	174.4(2)
θ	85.57(2)	84.23(6)/86.74(7)[a]	87.15(6)	83.79(5)/86.28(6)[a]	87.35(6)

[a]One pyrazolyl ring in the cation is partially disordered at this temperature.

Table S3 Hydrogen bond parameters (Å , °) for the acetonitrile solvates of **1X₂** (X^- = BF_4^- or ClO_4^-). See Figures S1-S3 for the atom numbering scheme.

	N−H	H···X	N···X	N−H···X
1[BF_4]$_2$·2MeCN, 120 K				
N(18)−H(18)···F(46A)/F(46B)	0.88	1.99/2.28	2.825(3)/3.091(6)	158.6/154.0
N(38)−H(38)···F(51)	0.88	2.09	2.877(2)	148.2
1[BF_4]$_2$·MeCN, 200 K				
N(18)−H(18)···F(46A)/F(46B)	0.88	1.99/1.93	2.854(6)/2.808(14)	168.5/171.4
N(38)−H(38)···F(51A)/F(51B)/F(51C)	0.88	2.27/2.15/2.09	3.019(14)/2.892(18)/2.837(14)	143.3/142.2/ 141.7
1[BF_4]$_2$·MeCN, 125 K				
N(18)−H(18)···F(46)	0.88	1.99	2.860(8)	170.5
N(38)−H(38)···F(51)	0.88	2.06	2.872(8)	152.6
1[ClO_4]$_2$·MeCN, 200 K				
N(18)−H(18)···O(46A)/O(46B)/O(46C)	0.88	2.01/2.14/1.93	2.881(9)/2.997(10)/2.810(12)	167.9/164.4/177.9
N(38)−H(38)···O(51A)/O(51B)[a]	0.88	2.20/2.14	2.951(15)/2.881(12)	142.6/141.3
1[BF_4]$_2$·MeCN, 125 K				
N(18)−H(18)···O(46A)/O(46B)	0.88	2.09/2.01	2.947(9)/2.888(12)	163.4/177.7
N(38)−H(38)···O(51)	0.88	2.13	2.943(8)	153.4

[a]The 'C' disorder orientation for this anion does not have an O atom within hydrogen bonding distance of the complex.

1[BF$_4$]$_2$·MeCN

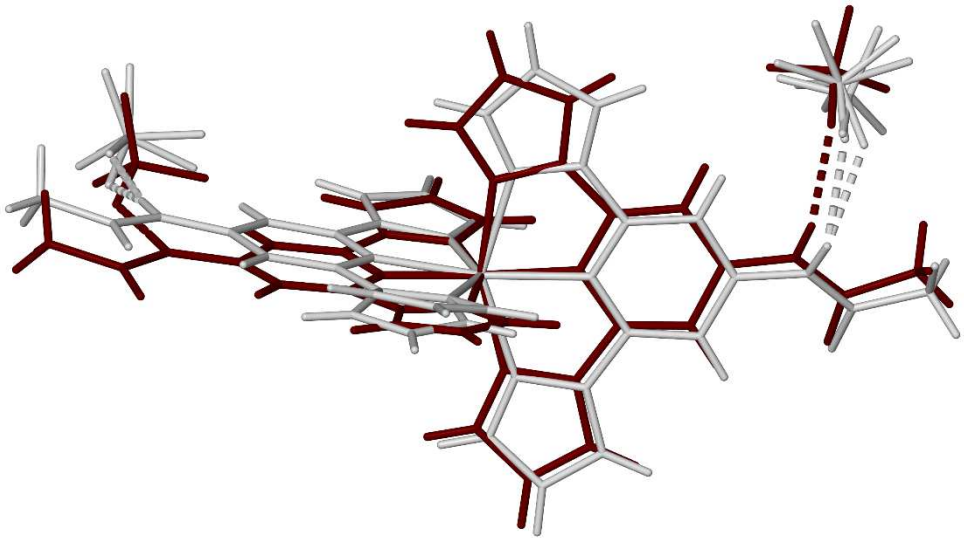

1[ClO$_4$]$_2$·MeCN

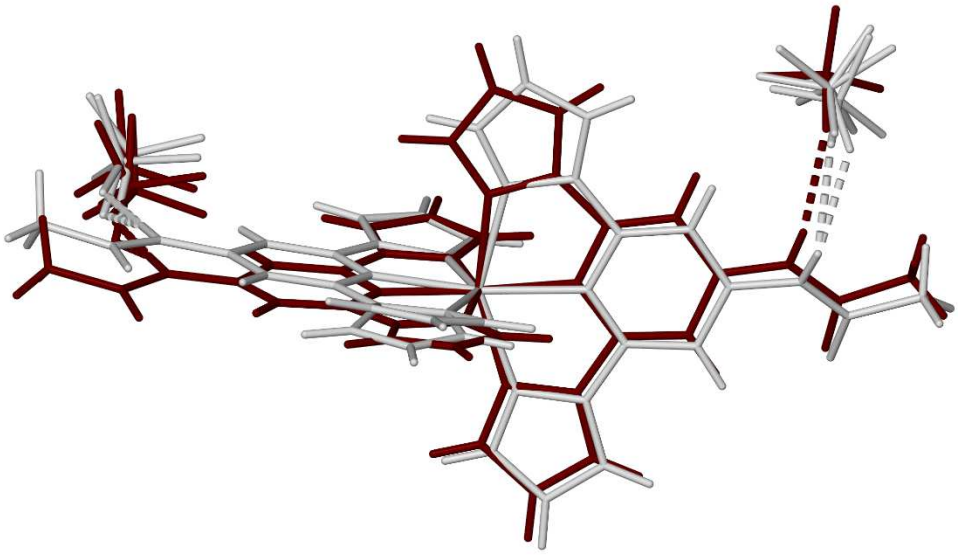

Figure S4 Overlays of the high-spin (white) and low-spin (brown) structures of the [FeL_2]X$_2$ assemblies in **1[BF$_4$]$_2$**·MeCN and **1[ClO$_4$]$_2$**·MeCN. The two models in each plot are centred on the Fe atom, and all orientations of disordered residues in the model are included in the plots.

The largest atomic displacements between the spin states involve the carboxamido group on the left of the plots, whose non-H atoms move by 0.9-1.0 Å during SCO in both salts. The central B atom of the BF_4^- ion hydrogen bonded to that group also translates by 0.6 Å during the transition. Displacement of that anion in the ClO_4^- salt is less clear, because it is disordered in both spin states.

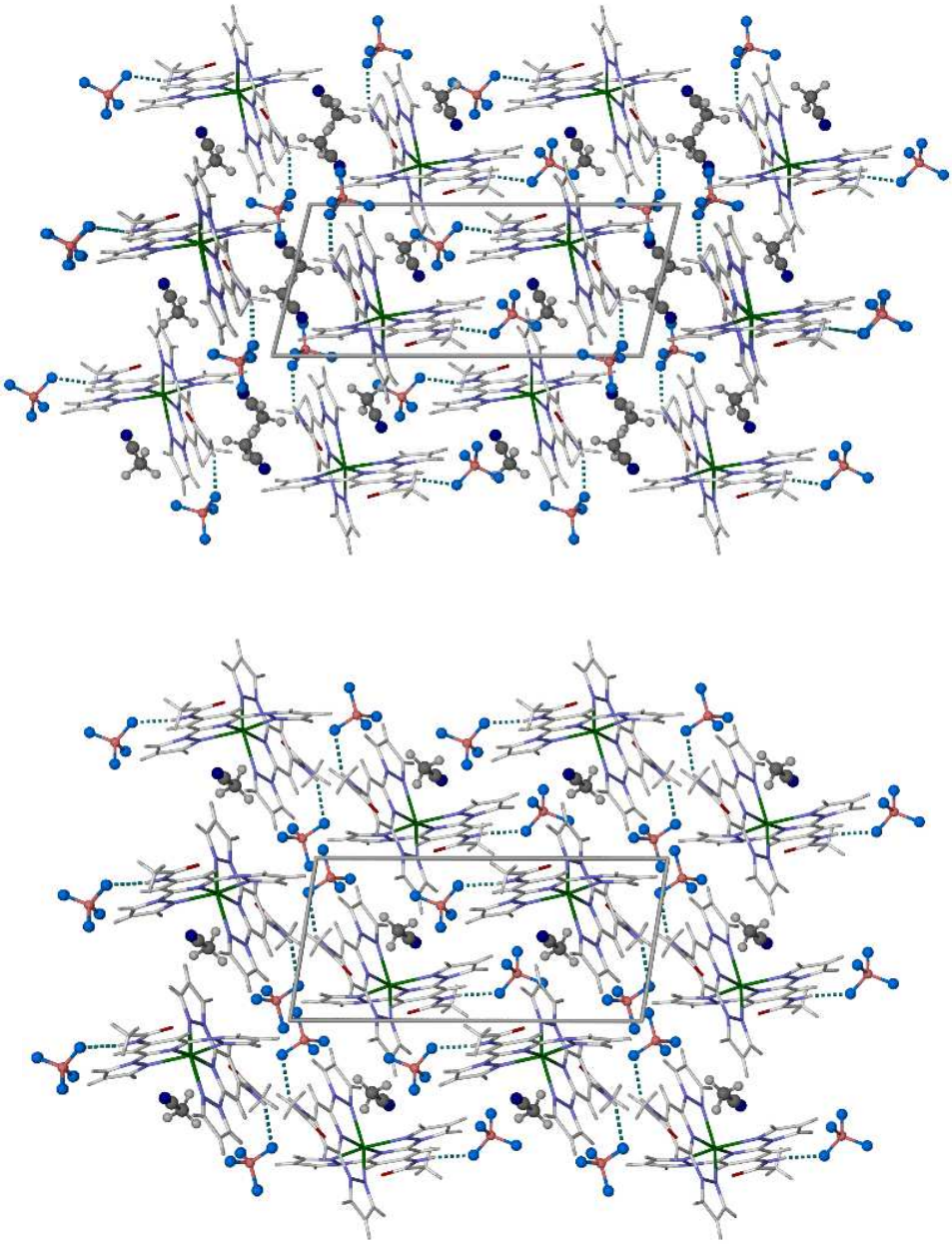

Figure S5 Packing diagrams of **1[BF$_4$]$_2$**·2MeCN (top) and the high-spin form of **1[BF$_4$]$_2$**·MeCN (bottom), viewed parallel to the [010] crystal vector with the *c* unit cell axis horizontal. Only one orientation of disordered residues is shown, and the cations are de-emphasised to highlight the differences between the structures.

Colour code: C{complex}, white; C{MeCN}, dark grey; H, pale grey; B, pink; F, cyan; Fe, green; N{complex}, pale blue; N{MeCN} dark blue; O, red.

The views are the same as Figure 1 of the main article, but without the highlighting colouration of the additional solvent in **1[BF$_4$]$_2$**·2MeCN.

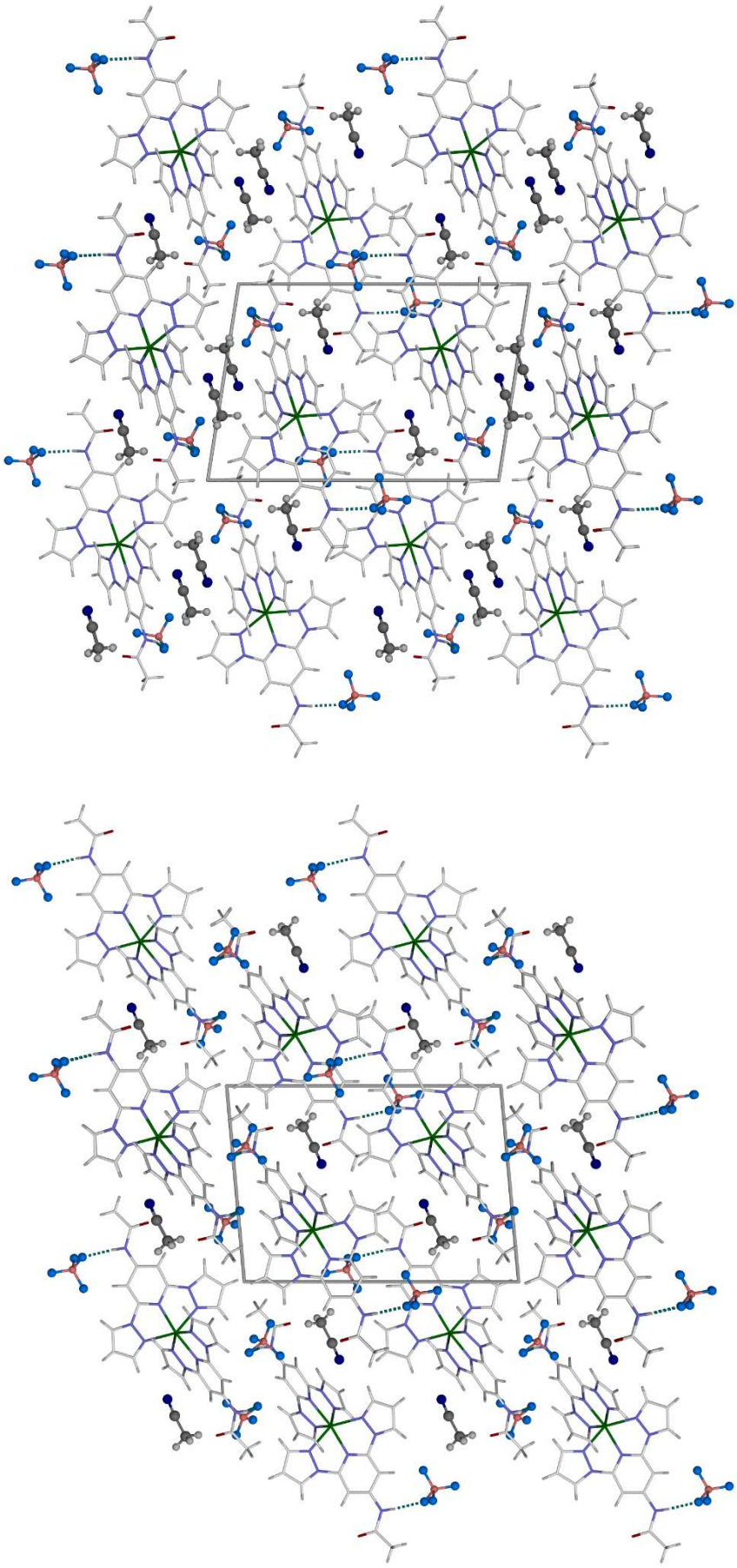

Figure S6 Alternative packing diagrams of **1[BF$_4$]$_2$**·2MeCN (top) and the high-spin form of **1[BF$_4$]$_2$**·MeCN (bottom), showing the opposite handedness of their triclinic unit cells. The view is parallel to the [100] crystal vector with *c* horizontal. Details as for Figure S5.

Table S4 Variable temperature unit cell parameters for **1[BF$_4$]$_2$**·MeCN.

T (K)	a (Å)	b (Å)	c (Å)	α (°)	β (°)	γ (°)	V (Å^3)
Cooling							
250	8.258(3)	12.561(4)	17.629(6)	83.59(3)	80.24(3)	80.85(3)	1772.4(10)
240	8.254(3)	12.545(4)	17.612(6)	83.55(3)	80.12(3)	80.77(3)	1766.7(10)
230	8.245(3)	12.550(4)	17.614(6)	83.51(3)	80.05(3)	80.74(3)	1764.9(10)
220	8.234(3)	12.561(5)	17.607(6)	83.40(3)	80.01(3)	80.74(3)	1763.0(11)
210	8.235(3)	12.557(4)	17.599(5)	83.36(3)	79.98(3)	80.72(3)	1761.3(10)
200	8.222(3)	12.552(4)	17.581(5)	83.29(3)	79.98(3)	80.76(3)	1756.2(10)
190	8.214(3)	12.546(4)	17.570(6)	83.33(3)	79.97(3)	80.75(3)	1752.6(11)
180	8.234(3)	12.359(5)	17.386(5)	83.29(3)	79.30(3)	84.77(3)	1722.2(11)
170	8.230(3)	12.351(4)	17.356(5)	83.25(3)	79.42(3)	84.95(3)	1718.1(10)
160	8.226(2)	12.342(4)	17.343(4)	83.24(2)	79.44(2)	85.07(2)	1715.3(8)
150	8.220(2)	12.342(3)	17.333(4)	83.18(2)	79.43(2)	85.04(2)	1712.7(8)
140	8.213(2)	12.343(3)	17.305(4)	83.19(2)	79.48(2)	85.15(2)	1708.9(8)
130	8.208(3)	12.343(4)	17.298(4)	83.11(2)	79.45(2)	85.19(2)	1706.9(8)
Warming							
140	8.213(2)	12.345(3)	17.311(4)	83.18(2)	79.43(2)	85.13(2)	1709.7(8)
150	8.224(2)	12.339(3)	17.328(4)	83.20(2)	79.41(2)	85.12(2)	1712.9(8)
160	8.228(2)	12.340(3)	17.342(4)	83.19(2)	79.44(2)	85.14(2)	1715.3(8)
170	8.241(3)	12.347(4)	17.352(5)	83.25(2)	79.41(2)	85.14(2)	1719.9(9)
180	8.262(3)	12.348(4)	17.368(5)	83.29(3)	79.24(3)	85.05(3)	1724.9(10)
190	8.263(3)	12.346(4)	17.375(5)	83.30(3)	79.23(3)	84.96(3)	1725.3(9)
200	8.2224(3)	12.550(4)	17.589(5)	83.29(3)	79.93(3)	80.76(3)	1756.6(11)
210	8.233(3)	12.549(4)	17.588(5)	83.39(3)	79.97(3)	80.82(3)	1759.4(10)
220	8.241(3)	12.545(5)	17.600(5)	83.45(3)	79.97(3)	80.76(3)	1761.5(11)
230	8.248(3)	12.556(5)	17.600(6)	83.49(3)	80.06(3)	80.80(3)	1765.3(11)
240	8.256(3)	12.552(4)	17.621(5)	83.58(3)	80.10(3)	80.84(3)	1769.3(10)
250	8.269(3)	12.560(4)	17.632(5)	83.65(3)	80.21(3)	80.90(3)	1775.3(10)
260	8.279(3)	12.566(4)	17.641(5)	83.69(3)	80.26(3)	80.92(3)	1779.6(10)

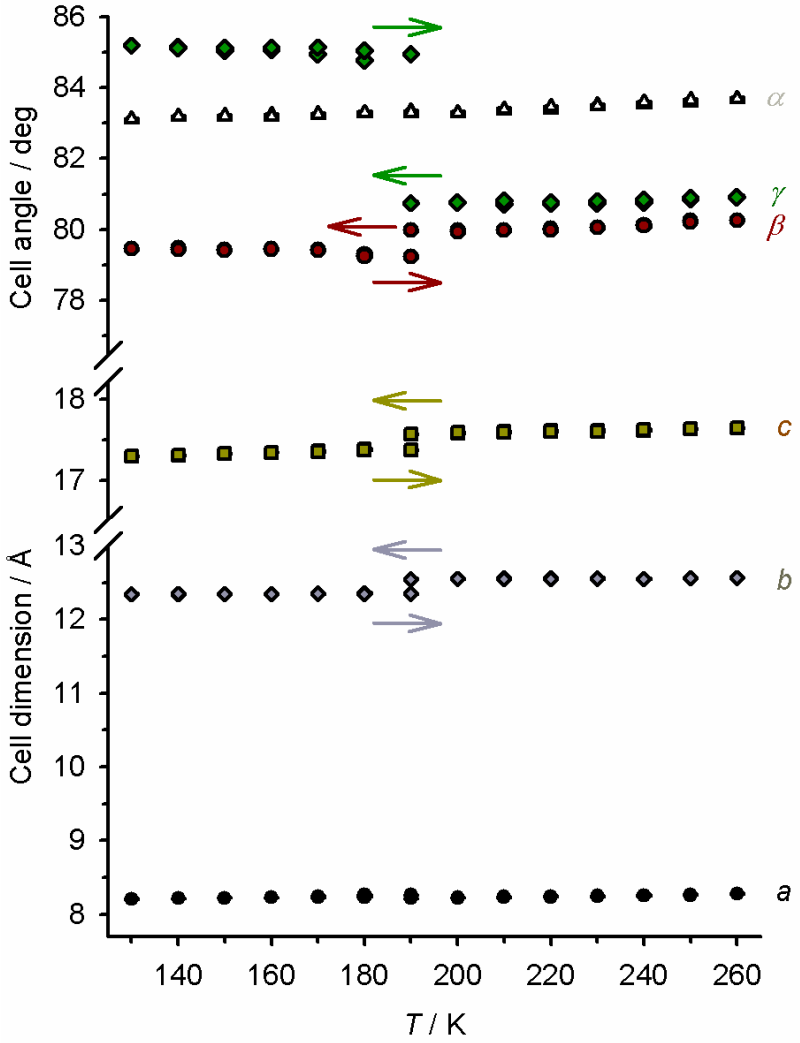

Figure S7 Variable temperature unit cell data for **1[BF$_4$]$_2$**·MeCN (Table S4). Data were collected in cooling and warming temperature ramps. Thermal hysteresis in the spin-transition is visible in *b*, *c*, β and γ.

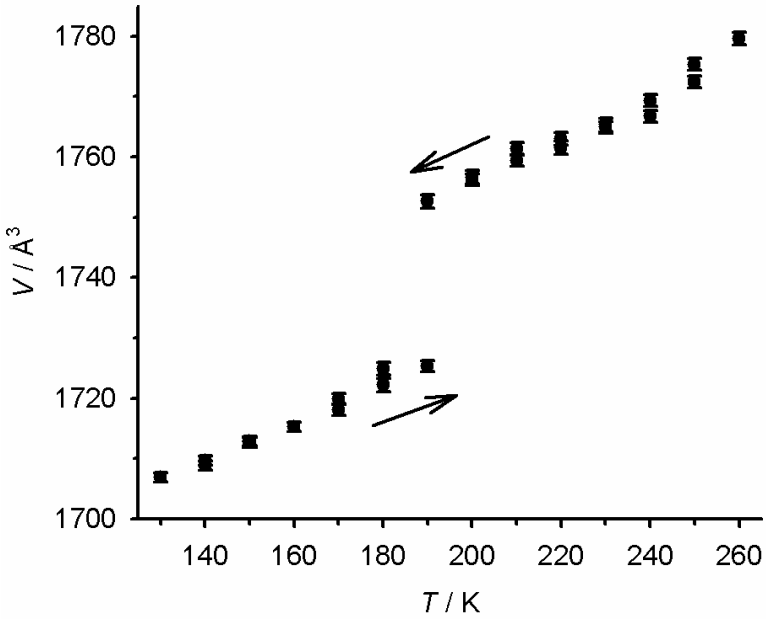

Figure S8 Variable temperature unit cell volumes for **1[BF$_4$]$_2$**·MeCN.

Table S5 Variable temperature unit cell parameters for **1[ClO$_4$]$_2$**·MeCN.

T (K)	a (Å)	b (Å)	c (Å)	α (°)	β (°)	γ (°)	V (Å^3)
Cooling							
240	8.2981(8)	12.630(5)	17.777(4)	82.88(2)	79.852(13)	80.730(18)	1801.3(8)
230	8.2951(8)	12.642(5)	17.768(4)	82.77(2)	79.776(14)	80.619(18)	1800.1(9)
220	8.2914(7)	12.637(5)	17.770(4)	82.79(2)	79.770(12)	80.622(17)	1798.9(8)
210	8.2889(8)	12.629(5)	17.761(4)	82.78(2)	79.715(13)	80.583(18)	1795.8(8)
200	8.2837(8)	12.628(5)	17.759(4)	82.69(3)	79.614(13)	80.506(18)	1793.1(9)
190	8.2880(10)	12.636(5)	17.738(4)	82.72(3)	79.571(14)	80.543(19)	1793.0(9)
180	8.2929(17)	12.631(5)	17.746(5)	82.68(3)	79.40(2)	80.55(2)	1793.3(10)
170	8.2814(13)	12.621(4)	17.721(5)	82.64(2)	79.426(17)	80.45(2)	1786.4(8)
160	8.284(7)	12.554(9)	17.807(11)	82.96(5)	78.59(8)	81.06(9)	1785(2)
150	8.2990(12)	12.387(4)	17.468(9)	81.69(3)	78.60(2)	85.606(19)	1739.7(11)
140	8.3048(17)	12.373(6)	17.496(4)	81.80(3)	78.563(19)	85.90(2)	1742.3(10)
130	8.2940(8)	12.379(4)	17.433(3)	81.67(2)	78.595(11)	85.668(16)	1734.0(7)
Warming							
140	8.3038(8)	12.395(5)	17.469(3)	81.69(2)	78.573(11)	85.680(16)	1741.9(7)
150	8.3084(8)	12.396(5)	17.486(3)	81.72(2)	78.584(11)	85.673(16)	1744.7(7)
160	8.3140(7)	12.372(4)	17.483(3)	81.77(2)	78.636(11)	85.638(15)	1742.9(7)
170	8.2722(10)	12.635(5)	17.716(5)	82.66(3)	79.508(16)	80.58(2)	1787.0(9)
180	8.2934(18)	12.649(5)	17.730(5)	82.73(3)	79.32(2)	80.49(2)	1793.8(10)
190	8.2697(12)	12.620(4)	17.748(8)	82.81(3)	79.65(2)	80.535(19)	1788.6(10)
200	8.293(2)	12.614(5)	17.730(6)	82.43(3)	79.65(3)	80.39(3)	1789.0(11)
210	8.3091(15)	12.645(5)	17.762(5)	82.68(3)	79.54(2)	80.50(2)	1801.0(10)
220	8.3005(9)	12.659(6)	17.753(4)	82.89(3)	79.688(14)	80.56(2)	1801.9(9)
230	8.3009(11)	12.561(7)	17.767(6)	82.59(4)	79.885(19)	80.71(3)	1790(10)
240	8.3085(9)	12.634(5)	17.790(4)	83.00(3)	79.842(15)	80.78(2)	1805.9(9)
250	8.316(10)	12.647(5)	17.804(4)	83.09(3)	79.865(15)	80.81(2)	1811.3(9)

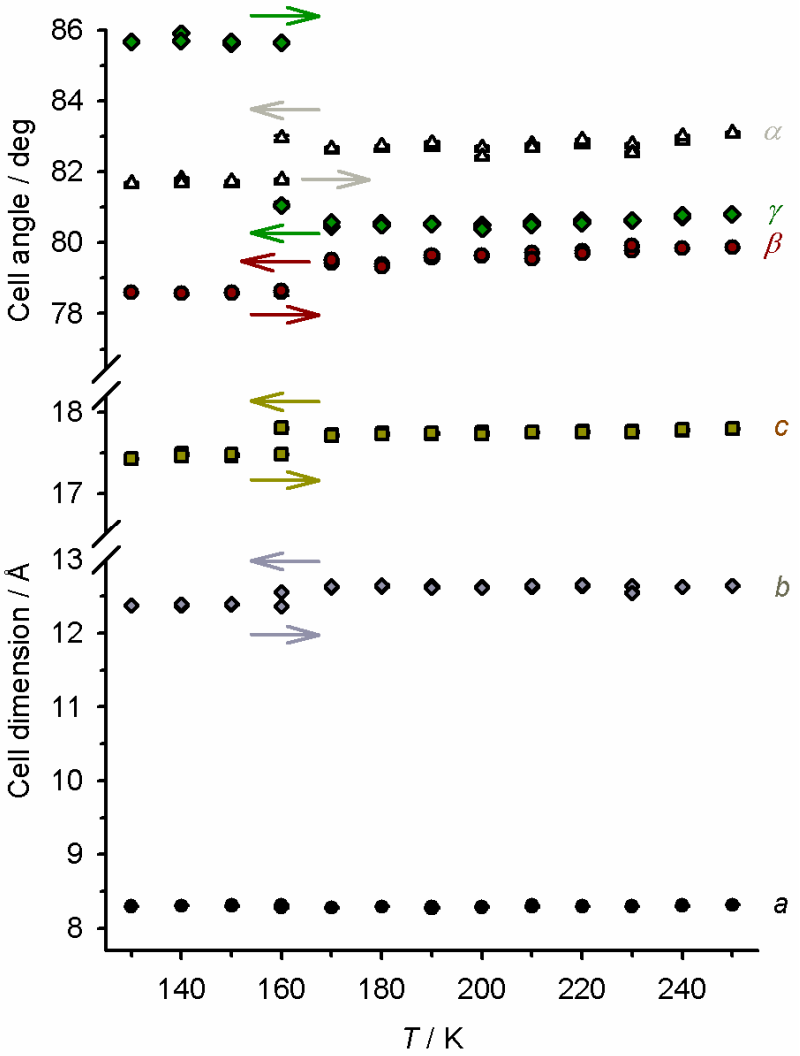

Figure S9 Variable temperature unit cell data for **1[ClO$_4$]$_2$**·MeCN (Table S5). Data were collected in cooling and warming temperature ramps. Thermal hysteresis in the spin-transition is visible in *b*, *c*, α and γ.

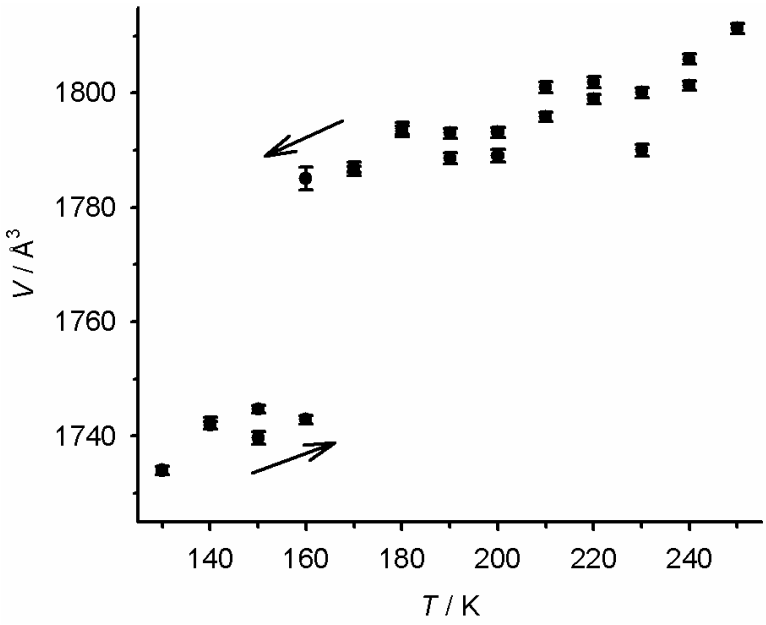

Figure S10 Variable temperature unit cell volumes for **1[ClO$_4$]$_2$**·MeCN.

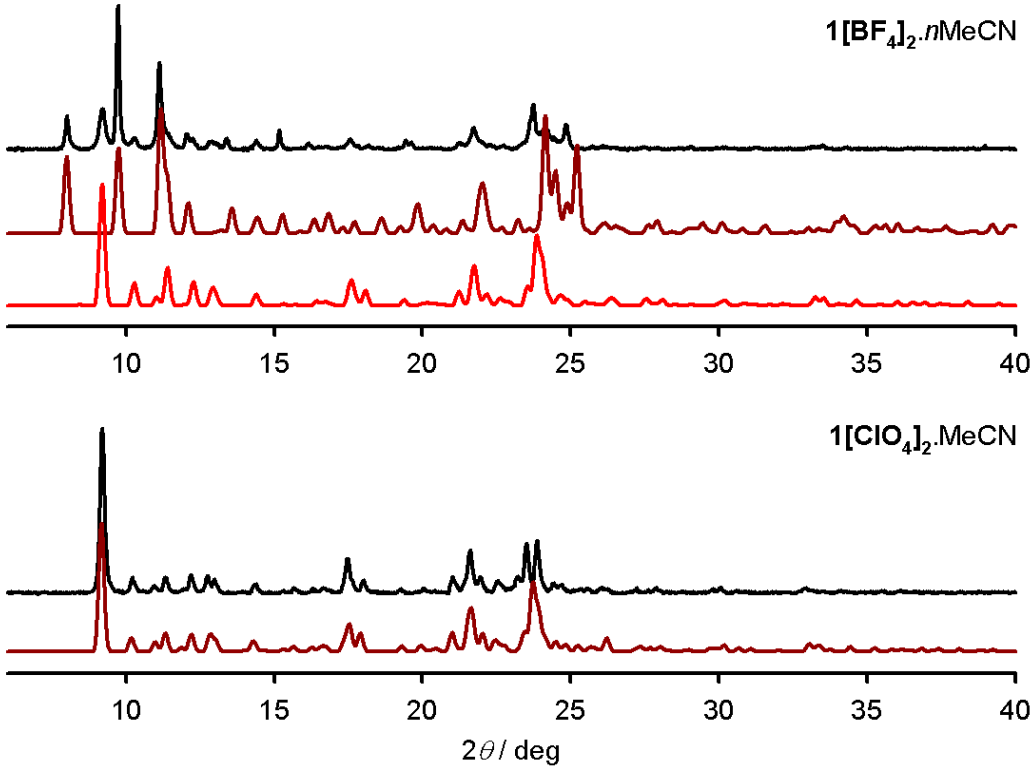

Figure S11 Measured (black) and simulated (red) room temperature X-ray powder diffraction data for the MeCN solvate materials.

Simulations for high-spin **1[BF$_4$]$_2$**·2MeCN (dark red) and SCO-active **1[BF$_4$]$_2$**·MeCN (pale red) are included. The sample of **1[BF$_4$]$_2$**·*n*MeCN is clearly a mixture of both compounds, with the high-spin **1[BF$_4$]$_2$**·2MeCN phase being the main component. That is consistent with its magnetic data when the material is protected from *in situ* solvent loss, where only *ca* 10 % of the sample exhibits the abrupt spin-transition undergone by single crystals of **1[BF$_4$]$_2$**·MeCN (Figure 2, main article).

There is excellent agreement between the measured and simulated data for **1[ClO$_4$]$_2$**·MeCN, showing that solvate is phase-pure.

While the peak positions should match well, some differences in the measured and simulated peak intensities are to be expected in measurements of this type, which were performed on polycrystalline materials rather than ideal powders.

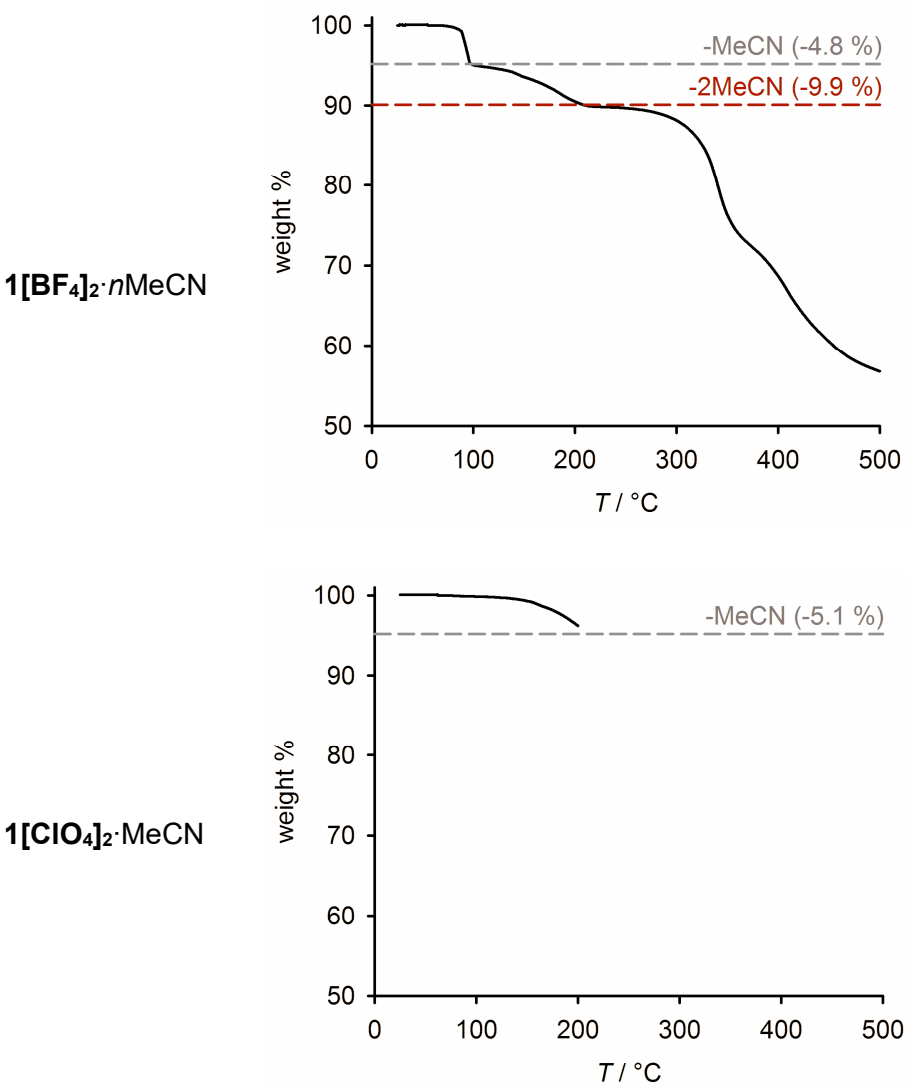

Figure S12 TGA data for **1[BF$_4$]$_2$**·*n*MeCN ($n \approx 2$) and **1[ClO]$_2$**·MeCN. The perchlorate salt was not heated above 200 °C because of its risk of detonation.

One equivalent of lattice solvent in **1[BF$_4$]$_2$**·*n*MeCN is lost abruptly at 95 °C, but the second equivalent of MeCN is lost much more gradually on further heating. The material only becomes fully desolvated at around 215 °C. The one equivalent of MeCN in **1[ClO]$_2$**·MeCN is also lost very gradually, with some solvent still being retained at 200 °C.

The high thermal stability of the **1[BF$_4$]$_2$**·MeCN and **1[BF$_4$]$_2$**·MeCN (*ie* $n = 1$) phases explains their stability to solvent loss inside the vacuum of the SQUID magnetometer cavity.

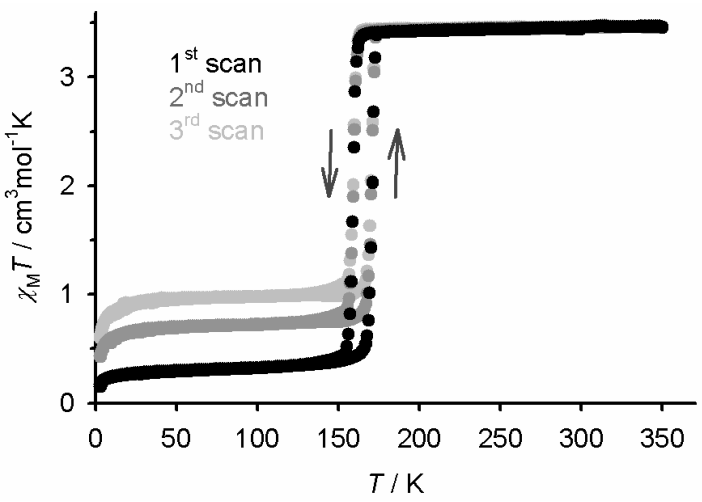

Figure S13 Variable temperature magnetic susceptibility data for **1[ClO$_4$]$_2$**·MeCN, at scan rate 5 K min^{-1}. Three scans were measured, in cooling and warming modes.

The fresh sample undergoes an abrupt spin transition to *ca* 85 % completeness, at $T_{½}\downarrow$ = 159 and $T_{½}\uparrow$ = 171 K. In contrast to **1[BF$_4$]$_2$**·*n*MeCN (*n* ≈ 1) however, the completeness of the transition slowly decreases upon repeated scanning, becoming 70 % complete on the third scan.

The sample of **1[ClO$_4$]$_2$**·MeCN is phase-pure by powder diffraction, unlike **1[BF$_4$]$_2$**·*n*MeCN which is a mixture of the *n* = 1 and *n* = 2 phases (Figure S11). Hence, we attribute this behaviour to gradual loss of MeCN from the sample upon repeated scanning inside the magnetometer, to ultimately generate a high-spin solvent-free material.

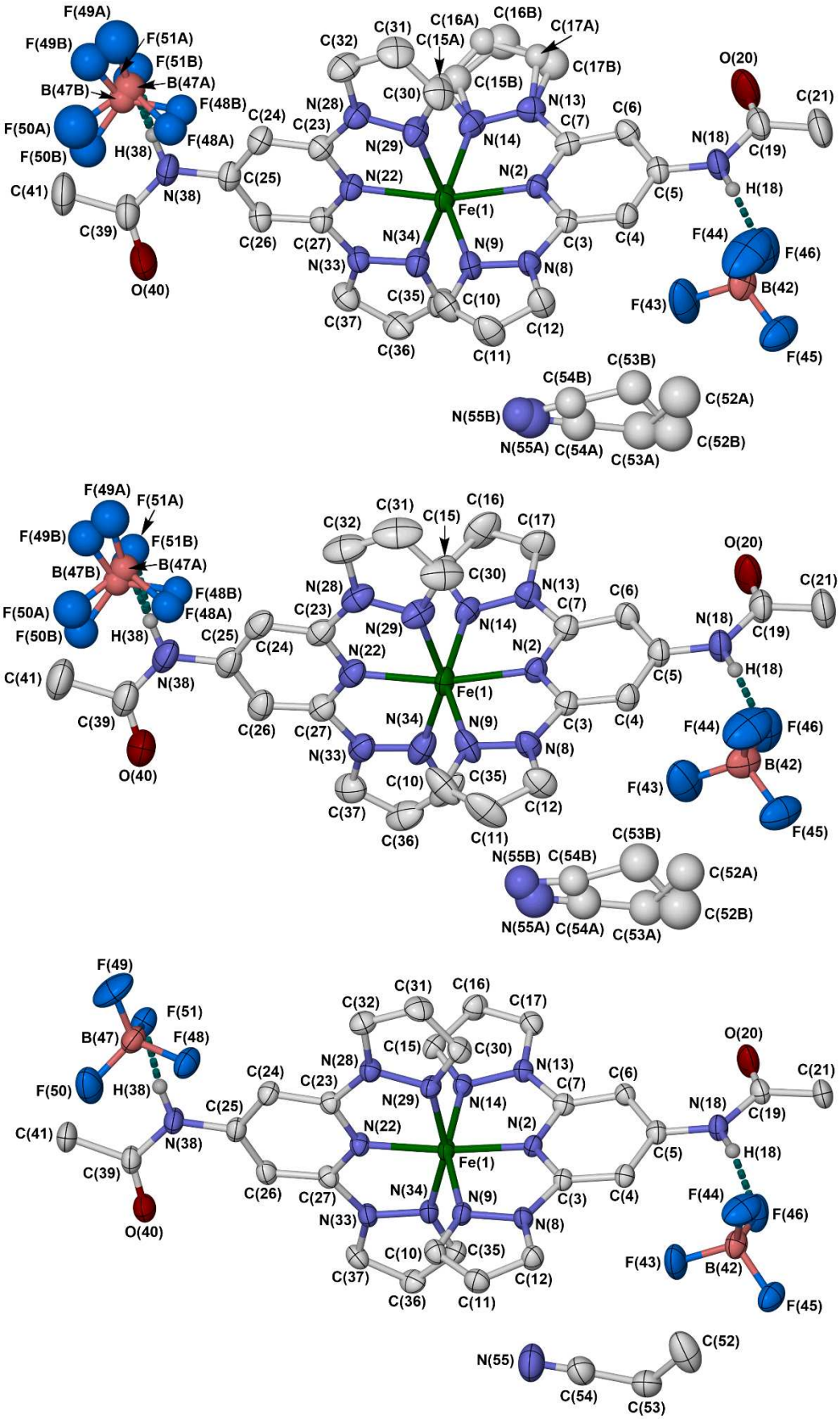

Figure S14 The asymmetric unit of **1[BF$_4$]$_2$**·EtCN at 200 K (high-spin, top), 187 K (mixed-spin, centre) and 160 K (low-spin, bottom), with the full atom numbering scheme. Displacement ellipsoids are at the 50 % probability level, and C-bound H atoms are omitted.

Colour code: C, white; H, pale grey; B, pink; F, cyan; Fe, green; N, blue; O, red.

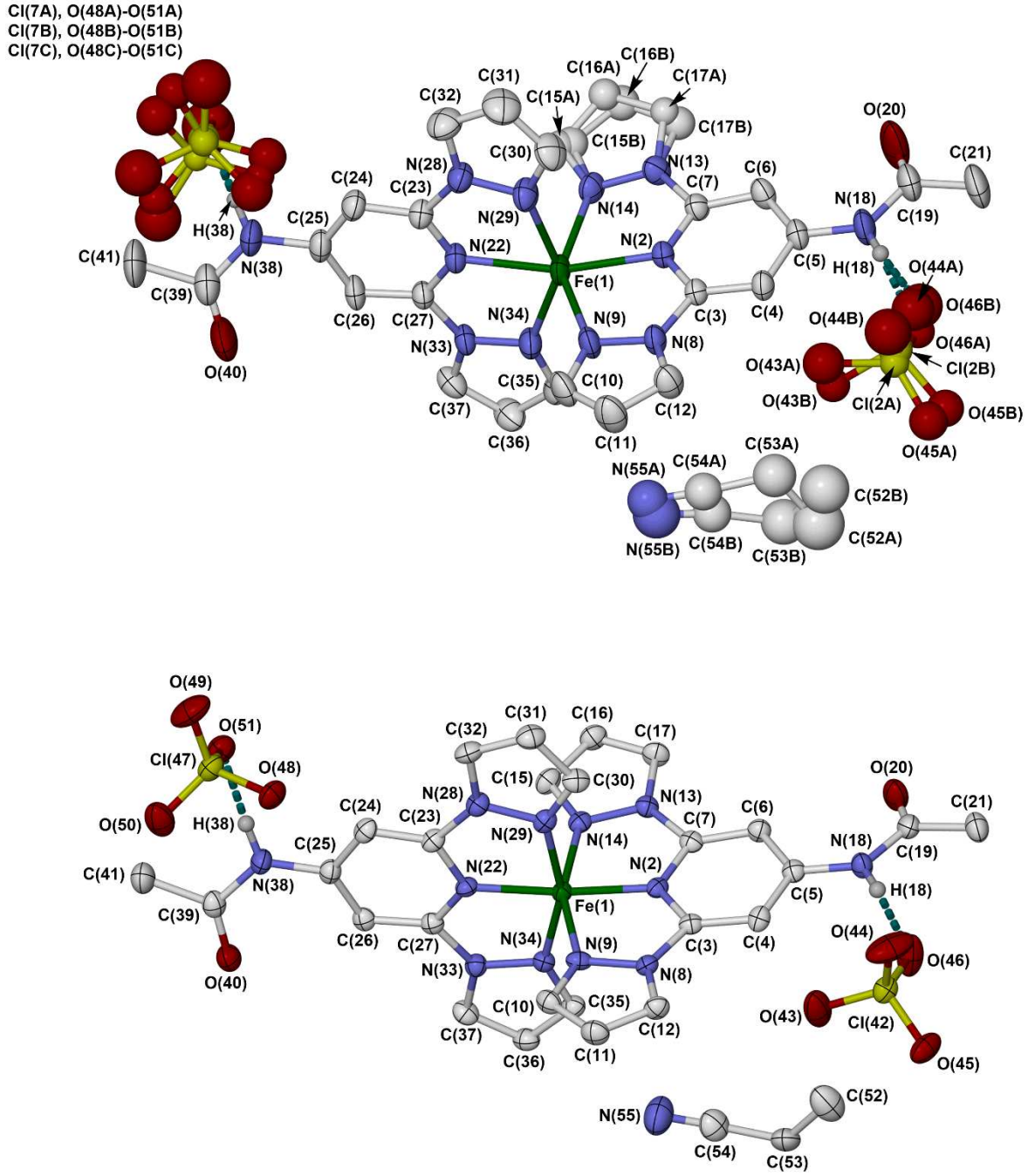

Figure S15 The asymmetric unit of phase 1 of **1[ClO$_4$]$_2$**·EtCN at 240 K (high-spin, top) and 120 K (low-spin, bottom), with the full atom numbering scheme. Displacement ellipsoids are at the 50 % probability level, and C-bound H atoms are omitted.

Colour code: C, white; H, pale grey; Cl, yellow; Fe, green; N, blue; O, red.

Atoms in the three-fold disordered anion in the higher temperature structure are not individually numbered, for clarity.

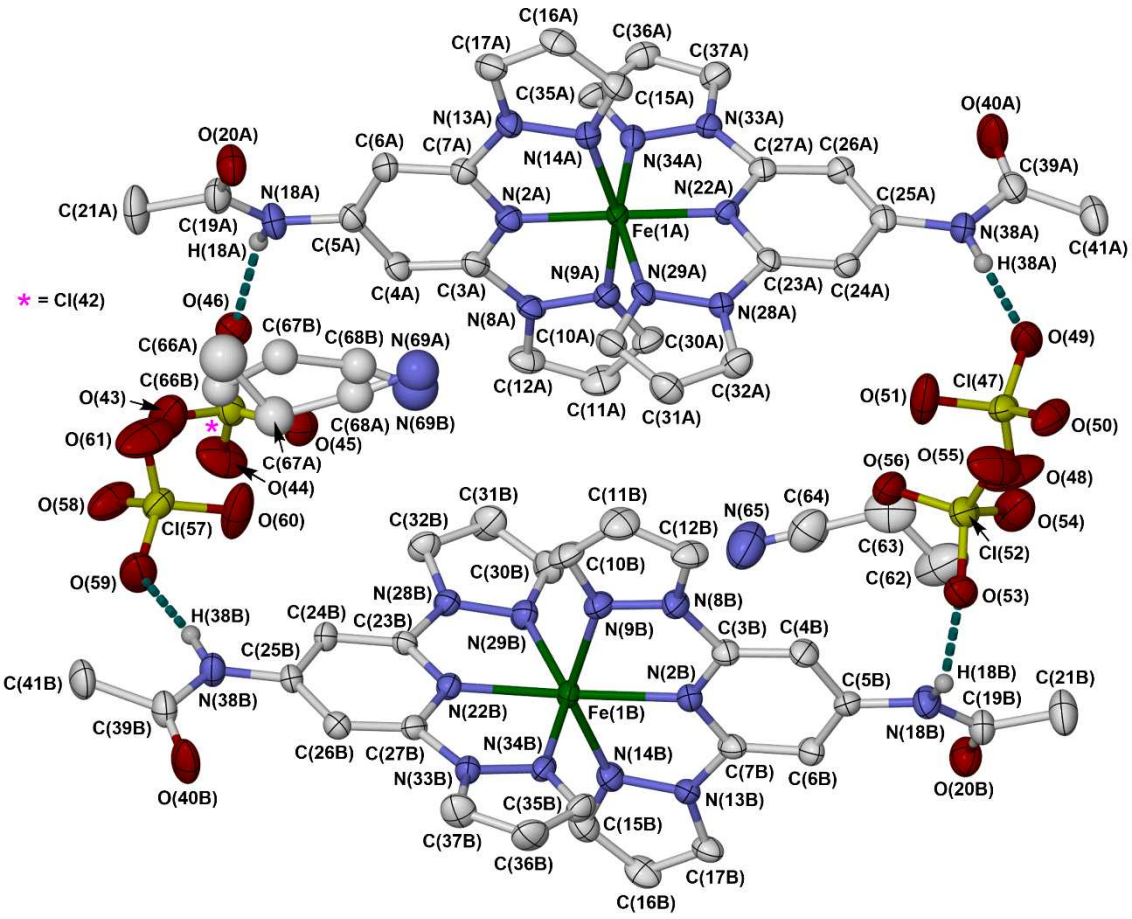

Figure S16 The asymmetric unit of phase 2 of **1[ClO$_4$]$_2$**·EtCN at 170 K, with the full atom numbering scheme. Displacement ellipsoids are at the 50 % probability level, and C-bound H atoms are omitted.

Colour code: C, white; H, pale grey; Cl, yellow; Fe, green; N, blue; O, red.

Molecule A is fully low-spin in this refinement, and molecule B is high-spin.

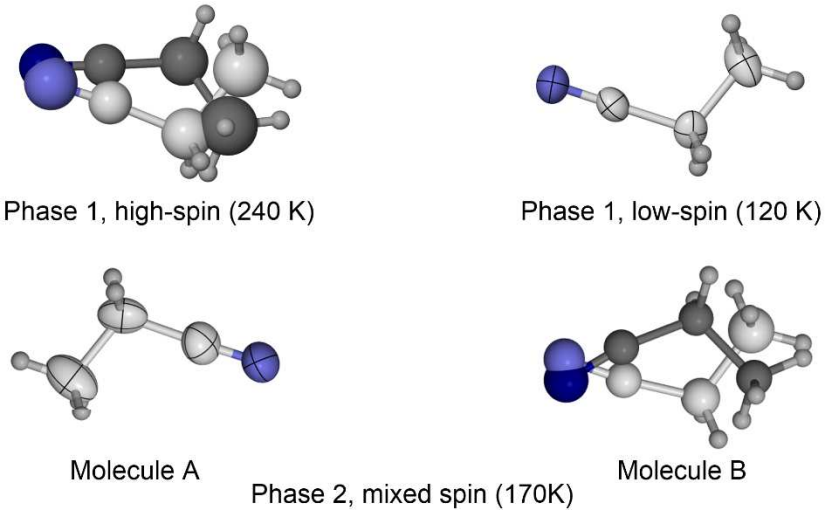

Figure S17 The orientations of the EtCN molecule in the different phases of **1[ClO$_4$]$_2$**·EtCN. Displacement ellipsoids are at the 50 % probability level, and C-bound H atoms are omitted.

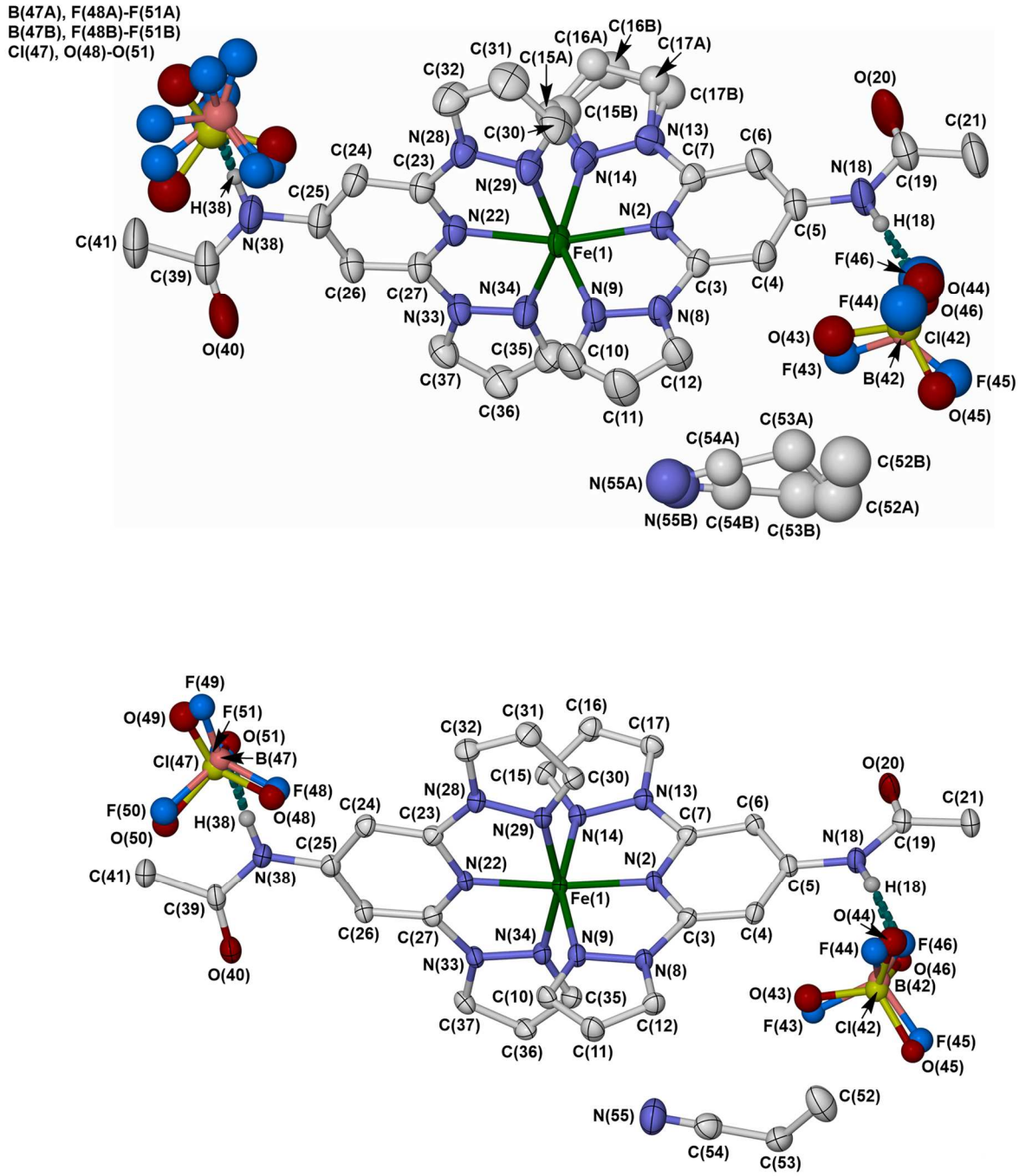

Figure S18 The asymmetric unit of phase 1 of **1**$[BF_4]_{0.9}[ClO_4]_{1.1}$·EtCN at 250 K (high-spin, top) and 125 K (low-spin, bottom), with the full atom numbering scheme. Displacement ellipsoids are at the 50 % probability level, and C-bound H atoms are omitted.

Colour code: C, white; H, pale grey; B, pink; Cl, yellow; F, cyan; Fe, green; N, blue; O, red.

Atoms in the three-fold disordered anion in the higher temperature structure are not individually numbered, for clarity.

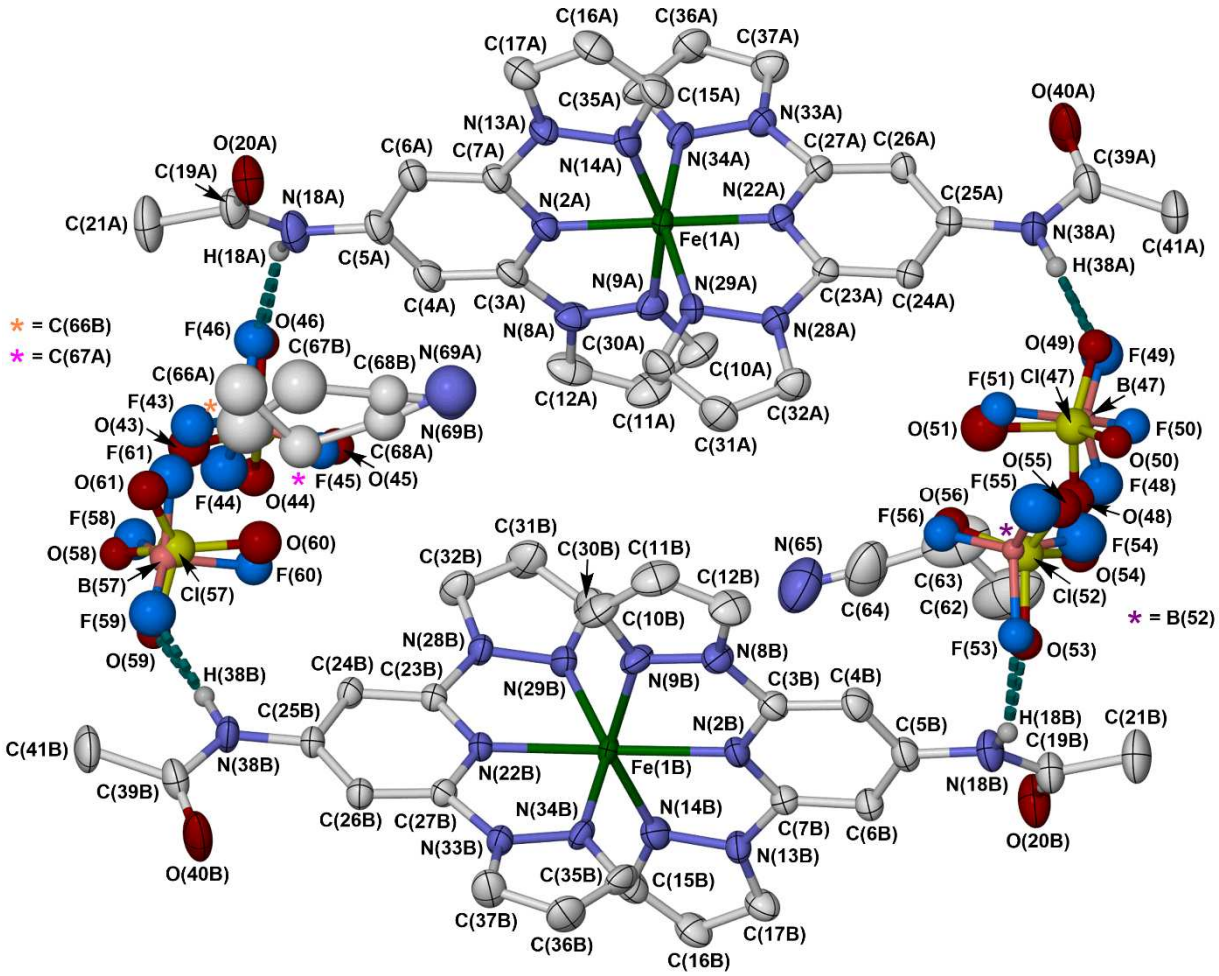

Figure S19 The asymmetric unit of the mixed-spin phase 2 of **1[BF$_4$]$_{0.9}$[ClO$_4$]$_{1.1}$**·EtCN at 180 K, with the full atom numbering scheme. Displacement ellipsoids are at the 50 % probability level, and C-bound H atoms are omitted.

Colour code: C, white; H, pale grey; B, pink; Cl, yellow; F, cyan; Fe, green; N, blue; O, red.

Molecule A is fully low-spin in this refinement, and molecule B is high-spin.

Table S6 Selected bond lengths, angles and other structural parameters (Å , °, Å^3) for the propionitrile solvates of **1X$_2$** (X^- = BF_4^- or ClO_4^-). See Figures S14-S19 for the atom numbering scheme, while definitions of V_{Oh}, Σ, Θ, φ and θ are given on page S10.

	1[BF$_4$]$_2$·EtCN			**1[ClO$_4$]$_2$**·EtCN			
T / K	200	187	160	240	170[b]		120
					Molecule A	Molecule B	
Fe(1)–N(2)	2.109(3)	2.038(3)	1.909(3)	2.117(4)	1.896(5)	2.121(5)	1.906(4)
Fe(1)–N(9)	2.179(3)	2.112(4)	1.997(4)	2.181(4)	1.974(5)	2.183(5)	1.992(3)
Fe(1)–N(14)	2.161(3)	2.081(3)	1.957(4)	2.179(4)	2.000(5)	2.173(5)	1.960(4)
Fe(1)–N(22)	2.121(3)	2.056(3)	1.910(4)	2.131(4)	1.907(5)	2.106(5)	1.904(4)
Fe(1)–N(29)	2.197(3)	2.112(4)	1.973(4)	2.204(5)	1.990(5)	2.173(5)	1.974(4)
Fe(1)–N(34)	2.175(3)	2.113(5)	1.987(4)	2.180(4)	1.962(5)	2.143(5)	1.991(4)
N(2)–Fe(1)–N(9)	73.64(10)	75.70(12)	79.78(15)	73.29(14)	79.8(2)	73.31(19)	79.76(15)
N(2)–Fe(1)–N(14)	73.50(10)	75.65(12)	79.47(15)	73.15(14)	79.8(2)	73.30(19)	79.85(15)
N(2)–Fe(1)–N(22)	165.76(11)	168.26(14)	173.79(18)	165.13(16)	173.4(2)	165.2(2)	174.36(14)
N(2)–Fe(1)–N(29)	95.44(11)	95.93(14)	95.99(16)	95.27(15)	104.9(2)	116.15(19)	95.96(15)
N(2)–Fe(1)–N(34)	118.30(11)	113.85(13)	105.04(16)	119.07(15)	95.9(2)	95.86(19)	104.73(15)
N(9)–Fe(1)–N(14)	147.12(11)	151.34(13)	159.25(15)	146.44(14)	159.6(2)	146.17(19)	159.60(15)
N(9)–Fe(1)–N(22)	115.16(11)	112.19(13)	104.70(16)	115.94(15)	95.1(2)	95.25(19)	104.28(15)
N(9)–Fe(1)–N(29)	94.79(12)	94.17(14)	92.35(17)	95.09(17)	91.5(2)	95.4(2)	92.13(14)
N(9)–Fe(1)–N(34)	96.91(11)	94.18(14)	95.96(17)	95.42(17)	89.6(2)	87.63(19)	92.42(14)
N(14)–Fe(1)–N(22)	95.61(12)	96.00(13)	92.36(17)	96.88(15)	105.3(2)	118.58(19)	96.04(15)
N(14)–Fe(1)–N(29)	87.33(12)	87.91(14)	89.38(17)	87.65(17)	93.3(2)	94.4(2)	89.60(14)
N(14)–Fe(1)–N(34)	100.67(12)	98.11(14)	93.41(17)	101.00(17)	92.9(2)	100.97(19)	93.10(14)
N(22)–Fe(1)–N(29)	73.24(11)	75.26(15)	79.66(17)	72.92(15)	79.19(19)	73.53(19)	80.08(15)
N(22)–Fe(1)–N(34)	73.25(11)	75.09(14)	79.30(16)	73.07(15)	79.9(2)	73.88(19)	79.22(15)
N(29)–Fe(1)–N(34)	146.24(11)	150.20(15)	158.95(15)	145.66(15)	159.1(2)	147.40(19)	159.29(15)
V_{Oh}	12.058(11)	11.177(12)	9.608(12)	12.138(15)	9.600(15)	11.910(18)	9.604(11)
Σ	155.9(4)	134.8(5)	92.2(6)	158.6(5)	90.6(7)	155.0(6)	90.2(5)
Θ	499	432	300	510	296	499	295
ϕ	165.76(11)	168.26(14)	173.79(18)	165.13(16)	173.4(2)	165.2(2)	174.36(14)
θ	83.75(5)/84.77(5)[a]	85.20(4)	87.38(5)	83.31(8)/84.93(8)[a]	88.76(4)	83.58(4)	87.91(4)

[a]One pyrazolyl ring in the cation is partially disordered at this temperature. [b]The crystal has transformed to a mixed-spin intermediate phase at this temperature, with two unique molecules in its asymmetric unit.

Table S6 continued.

	1$[BF_4]_{0.9}[ClO_4]_{1.1}$·EtCN			
T / K	250	180[b]		125
		Molecule A	Molecule B	
Fe(1)–N(2)	2.119(3)	1.920(3)	2.108(3)	1.902(2)
Fe(1)–N(9)	2.195(3)	1.995(3)	2.180(3)	1.993(2)
Fe(1)–N(14)	2.172(3)	2.000(3)	2.162(4)	1.960(2)
Fe(1)–N(22)	2.124(3)	1.927(3)	2.091(3)	1.907(2)
Fe(1)–N(29)	2.210(3)	2.008(3)	2.162(3)	1.969(3)
Fe(1)–N(34)	2.176(3)	1.982(3)	2.133(3)	1.991(3)
N(2)–Fe(1)–N(9)	73.25(11)	79.27(13)	73.61(12)	79.74(10)
N(2)–Fe(1)–N(14)	73.23(11)	78.95(12)	73.55(12)	79.62(10)
N(2)–Fe(1)–N(22)	165.47(12)	172.77(13)	166.31(12)	174.23(10)
N(2)–Fe(1)–N(29)	95.51(12)	105.62(12)	115.18(12)	95.84(10)
N(2)–Fe(1)–N(34)	118.63(12)	96.06(12)	96.06(11)	104.40(10)
N(9)–Fe(1)–N(14)	146.47(12)	158.22(13)	146.83(12)	159.36(10)
N(9)–Fe(1)–N(22)	115.67(12)	95.28(13)	96.25(12)	104.41(10)
N(9)–Fe(1)–N(29)	95.17(13)	92.16(13)	95.08(13)	91.97(10)
N(9)–Fe(1)–N(34)	95.51(13)	89.11(13)	87.74(12)	92.66(10)
N(14)–Fe(1)–N(22)	97.10(12)	106.46(12)	116.92(12)	96.14(10)
N(14)–Fe(1)–N(29)	87.54(14)	93.30(13)	94.60(13)	89.68(10)
N(14)–Fe(1)–N(34)	100.81(13)	93.57(13)	100.23(12)	92.88(10)
N(22)–Fe(1)–N(29)	72.88(12)	79.16(12)	74.20(11)	80.14(10)
N(22)–Fe(1)–N(34)	73.25(12)	78.99(12)	73.98(11)	79.60(10)
N(29)–Fe(1)–N(34)	145.85(12)	158.14(12)	148.18(11)	159.73(10)
V_{Oh}	12.170(12)	9.807(10)	11.824(11)	9.595(8)
Σ	158.3(4)	97.0(4)	151.2(4)	89.5(3)
Θ	508	314	486	293
ϕ	165.47(12)	172.77(13)	166.31(12)	174.23(10)
θ	83.36(6)/84.97(6)[a]	88.02(4)	84.28(4)	88.03(3)

[a]One pyrazolyl ring in the cation is partially disordered at this temperature. [b]The crystal has transformed to a mixed-spin intermediate phase at this temperature, with two unique molecules in its asymmetric unit.

Table S7 Hydrogen bond parameters (Å , °) for the propionitrile solvates of **1X$_2$** (X^- = BF_4^- or ClO_4^-). See Figures S14-S19 for the atom numbering scheme.

	N−H	H···X	N···X	N−H···X
1[BF$_4$]$_2$·EtCN, 200 K (phase 1)				
N(18)−H(18)···F(46)	0.88	1.95	2.829(4)	174.7
N(38)−H(38)···F(51A)/F(51B)	0.88	2.02/2.24	2.808(9)/3.023(9)	148.0/148.1
1[BF$_4$]$_2$·EtCN, 187 K (phase 1)				
N(18)−H(18)···F(46)	0.88	1.96	2.838(5)	174.2
N(38)−H(38)···F(51A)/F(51B)	0.88	1.97/2.27	2.776(9)/3.065(9)	150.8/151.0
1[BF$_4$]$_2$·EtCN, 160 K (phase 1)				
N(18)−H(18)···F(46)	0.88	1.98	2.848(5)	170.7
N(38)−H(38)···F(51)	0.88	2.06	2.890(6)	156.1
1[ClO$_4$]$_2$·EtCN, 240 K (phase 1)				
N(18)−H(18)···O(46A)/O(46B)	0.87	2.07/1.96	2.930(10)/2.832(13)	167.5/174.8
N(38)−H(38)···O(51A)/O(51B)/O(51C)	0.87	2.09/2.08/2.39	2.881(18)/2.89(3)/3.172(18)	150.2/154.2/150.0
1[ClO$_4$]$_2$·EtCN, 170 K (phase 2)				
N(18A)−H(18A)···O(46)	0.88	2.11	2.941(8)	157.2
N(38A)−H(38A)···O(49)	0.88	2.05	2.923(8)	173.8
N(18B)−H(18B)···O(53)	0.88	2.15	2.963(7)	153.1
N(38B)−H(38B)···O(59)	0.88	1.99	2.863(8)	169.3
1[ClO$_4$]$_2$·EtCN, 240 K (phase 1)				
N(18)−H(18)···O(46)	0.88	2.02	2.895(5)	172.4
N(38)−H(38)···O(51)	0.88	2.11	2.949(5)	160.3
1[BF$_4$]$_{0.9}$[ClO$_4$]$_{1.1}$·EtCN, 250 K (phase 1)				
N(18)−H(18)···F(46)/O(46)	0.87	1.99/2.03	2.855(9)/2.883(7)	175.3/167.4
N(38)−H(38)···F(51B)/O(51)[a]	0.87	2.16/2.08	2.915(17)/2.870(9)	144.5/150.5

[a]The 'A' disorder orientation for the disordered partial BF_4^- ion does not have an F atom within hydrogen bonding distance of the complex.

Table S7 continued.

	N−H	H···X	N···X	N−H···X
1[BF_4]$_{0.9}$[ClO_4]$_{1.1}$·EtCN, 180 K (phase 2)				
N(18A)−H(18A)···F(46)/O(46)	0.88	1.98/2.17	2.793(10)/2.995(8)	154.1/156.6
N(38A)−H(38A)···F(49)/O(49)	0.88	1.94/2.08	2.820(7)/2.948(7)	177.5/168.5
N(18B)−H(18B)···F(53)/O(53)	0.88	2.27/2.02	3.078(9)/2.823(8)	152.6/152.0
N(38B)−H(38B)···F(59)/O(59)	0.88	1.97/2.01	2.849(8)/2.869(7)	178.4/165.4
1[BF_4]$_{0.9}$[ClO_4]$_{1.1}$·EtCN, 125 K (phase 1)				
N(18)−H(18)···F(46)/O(46)	0.88	1.98/2.05	2.855(5)/2.915(5)	176.3/165.9
N(38)−H(38)···F(51)/O(51)	0.88	2.04/2.10	2.873(9)/2.942(8)	157.0/159.0

[a]The 'A' disorder orientation for the disordered partial BF_4^- ion does not have an F atom within hydrogen bonding distance of the complex.

Table S8 Variable temperature unit cell parameters for **1[BF$_4$]$_2$**·EtCN.

T (K)	a (Å)	b (Å)	c (Å)	α (°)	β (°)	γ (°)	V (Å^3)
Cooling							
260	8.2835(10)	12.6087(15)	17.9312(18)	84.201(9)	80.314(9)	81.312(10)	1819.4(4)
240	8.2629(8)	12.6120(12)	17.8983(14)	84.324(7)	80.263(7)	81.187(8)	1811.5(3)
220	8.2482(8)	12.6200(11)	17.8723(16)	84.235(7)	80.235(8)	81.190(7)	1806.5(3)
210	8.2420(7)	12.6206(11)	17.8593(15)	84.194(7)	80.198(7)	81.187(7)	1803.6(3)
200	8.2348(7)	12.6153(10)	17.8416(15)	84.147(7)	80.178(7)	81.244(7)	1799.5(3)
195	8.2329(7)	12.6131(10)	17.8289(14)	84.106(7)	80.155(7)	81.293(7)	1797.5(3)
190	8.2806(8)	12.4978(11)	17.6711(16)	83.765(8)	79.401(8)	83.228(8)	1777.9(3)
180	8.3159(10)	12.3644(13)	17.5282(19)	83.513(9)	78.886(9)	84.829(9)	1752.8(3)
170	8.3225(10)	12.3537(14)	17.494(2)	83.490(9)	78.839(10)	84.806(10)	1748.9(4)
150	8.3032(5)	12.3592(13)	17.4809(14)	83.457(8)	78.769(6)	84.970(7)	1744.1(3)
Warming							
170	8.3192(10)	12.3543(14)	17.502(2)	83.478(9)	78.830(10)	84.822(10)	1749.1(4)
180	8.3157(10)	12.3575(15)	17.5380(18)	83.498(9)	78.859(9)	85.040(10)	1753.0(3)
190	8.2985(9)	12.5008(14)	17.674(2)	83.546(9)	79.384(10)	83.172(9)	1781.6(3)
200	8.2377(8)	12.6110(12)	17.8350(17)	84.100(8)	80.112(8)	81.272(8)	1798.5(3)
210	8.2418(8)	12.6301(17)	17.8566(16)	84.274(9)	80.143(8)	81.195(10)	1804.6(3)
220	8.2448(10)	12.6265(15)	17.873(2)	84.061(10)	80.155(10)	81.224(10)	1806.1(4)
240	8.2713(10)	12.6162(13)	17.898(2)	84.272(9)	80.138(10)	81.200(9)	1813.2(4)
260	8.2839(10)	12.6097(15)	17.929(2)	84.373(10)	80.205(10)	81.273(10)	1819.1(4)

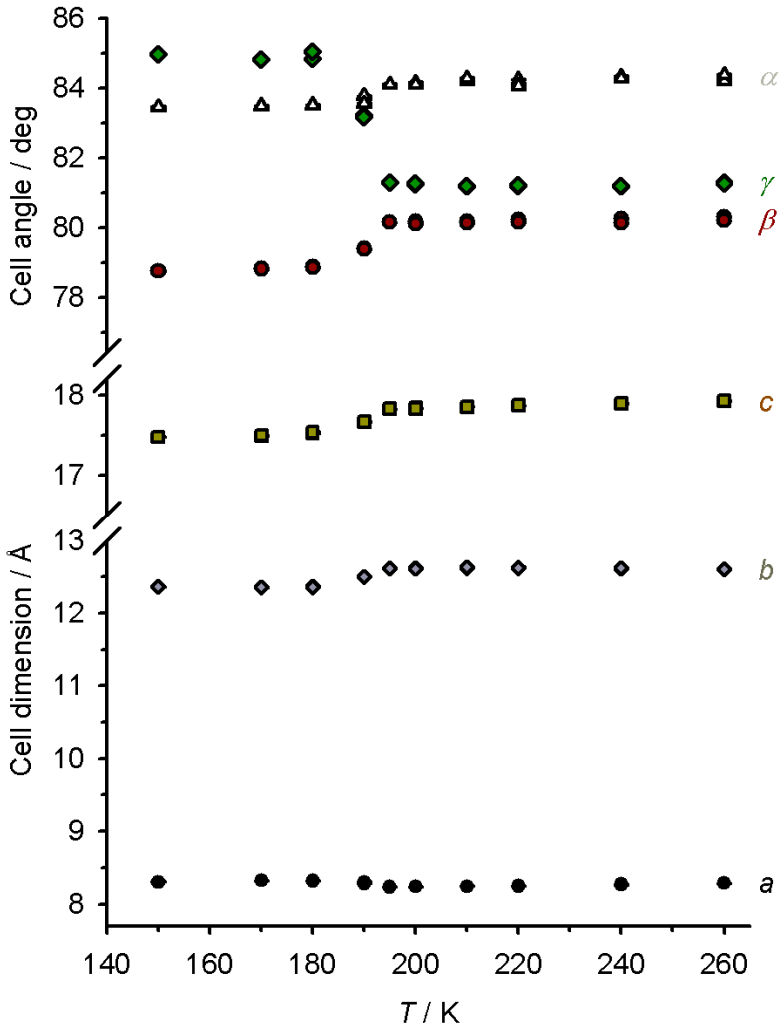

Figure S20 Variable temperature unit cell data for **1[BF$_4$]$_2$**·EtCN (Table S8). Data were collected in cooling and warming temperature ramps. The two steps in the spin-transition detected in the magnetic measurements are not resolved in these data, and there is no evidence for a transformation to phase 2 at 190 K.

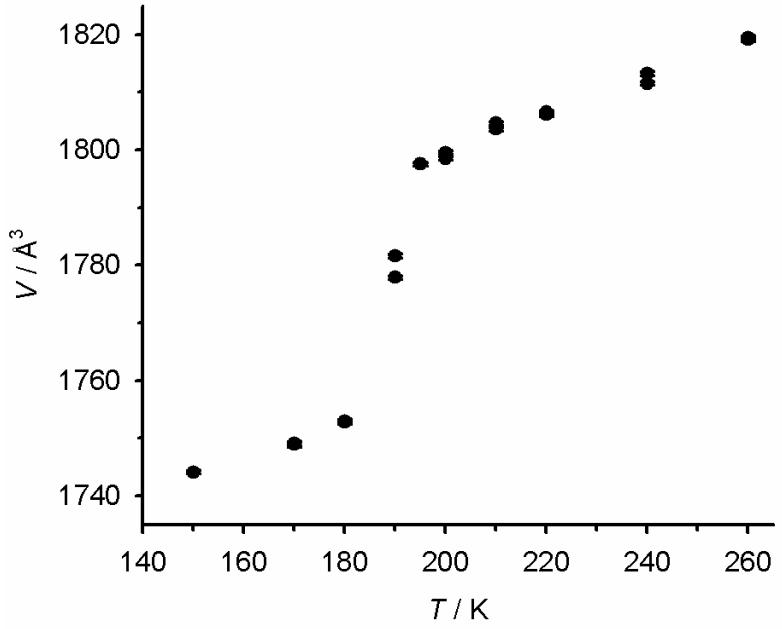

Figure S21 Variable temperature unit cell volumes for **1[BF$_4$]$_2$**·EtCN. Details as for Figure S20.

Table S9 Variable temperature unit cell parameters for **1[ClO$_4$]$_2$**·EtCN.

T (K)	a (Å)	b (Å)	c (Å)	α (°)	β (°)	γ (°)	V (Å^3)
Cooling							
250	8.3261(6)	12.6464(12)	18.1333(15)	83.748(7)	80.072(7)	80.820(8)	1850.2(3)
240	8.3254(4)	12.6603(8)	18.0999(9)	83.637(5)	79.989(4)	80.920(5)	1848.34(18)
230	8.3196(4)	12.6636(8)	18.0853(9)	83.585(5)	79.971(4)	80.902(5)	1845.71(18)
220	8.3099(4)	12.6630(4)	18.0692(9)	83.541(5)	79.956(4)	80.897(5)	1841.59(17)
210	8.3026(4)	12.6623(8)	18.0523(9)	83.513(5)	79.957(4)	80.873(5)	1837.98(17)
200	8.2963(4)	12.6619(8)	18.0336(9)	83.454(5)	79.927(4)	80.882(5)	1834.33(17)
190	8.2869(4)	12.6644(8)	18.0207(9)	83.419(5)	79.901(4)	80.891(5)	1831.13(17)
180	8.3179(7)	20.4444(14)	22.8327(15)	108.290(6)	98.604(6)	95.051(6)	3607.3(5)
170	8.3266(6)	20.3933(13)	22.8237(14)	108.169(5)	98.623(6)	95.300(6)	3600.6(4)
160	8.3275(7)	20.3613(12)	22.8049(13)	108.012(5)	98.639(6)	95.455(6)	3594.2(4)
150	8.3405(16)	20.2953(15)	22.8076(16)	107.818(6)	98.978(11)	95.856(11)	3584.1(8)
140	8.3395(11)	12.3802(13)	17.7141(18)	82.234(9)	78.620(10)	84.996(9)	1773.0(3)
120[a]	8.3410(3)	12.3849(4)	17.6860(3)	82.187(3)	78.664(3)	85.140(3)	1771.57(10)
Warming							
150	8.3405(16)	20.2953(15)	22.8076(16)	107.818(6)	98.978(11)	95.856(11)	3584.1(8)
160	8.3290(6)	20.3656(12)	22.8069(13)	108.043(5)	98.658(5)	95.479(5)	3594.6(4)
170	8.3302(6)	20.4001(12)	22.8201(14)	108.136(5)	98.665(6)	95.364(6)	3602.4(4)
180	8.3269(7)	20.4419(13)	22.8264(15)	108.243(6)	98.645(6)	95.169(6)	3609.1(4)
190	8.2780(5)	12.6703(9)	17.9997(10)	83.415(5)	79.964(5)	80.955(6)	1828.5(2)
200	8.2941(6)	12.6660(10)	18.0156(12)	83.428(6)	79.970(6)	80.921(6)	1832.9(2)
210	8.3010(6)	12.6628(10)	18.0375(12)	83.500(6)	79.997(6)	80.892(7)	1836.5(2)
220	8.3087(6)	12.6628(10)	18.0510(13)	83.527(6)	80.017(6)	80.918(7)	1839.8(2)
230	8.3163(7)	12.6632(10)	18.0668(13)	83.568(6)	80.039(6)	80.929(7)	1843.5(2)
240	8.3221(6)	12.6573(10)	18.0866(13)	83.608(6)	80.057(6)	80.940(7)	1846.2(2)
250	8.3361(10)	12.6409(13)	18.1125(19)	83.604(9)	79.969(9)	80.975(9)	1849.2(3)

[a]Unit cell from the single crystal structure determination at this temperature (which was collected from the same crystal used for this measurement).

Table S10 Variable temperature unit cell parameters for **1[BF$_4$]$_{0.9}$[ClO$_4$]$_{1.1}$**·EtCN. These data were measured in cooling mode only.

T (K)	a (Å)	b (Å)	c (Å)	α (°)	β (°)	γ (°)	V (Å^3)
240	8.2823(10)	12.630(3)	18.014(3)	83.96(2)	80.218(11)	81.108(17)	1828.7(6)
230	8.2739(9)	12.628(3)	18.005(3)	83.95(2)	80.220(11)	81.093(16)	1825.4(6)
220	8.2668(9)	12.632(3)	17.997(3)	83.917(19)	80.200(11)	81.112(16)	1823.5(6)
210	8.2633(9)	12.634(3)	17.990(3)	83.89(2)	80.132(11)	81.134(16)	1822.1(6)
200	8.2565(9)	12.631(3)	17.974(3)	83.83(2)	80.126(11)	81.152(16)	1818.5(6)
190	8.2446(10)	12.620(3)	17.955(4)	83.73(2)	80.081(13)	81.313(17)	1812.5(7)
180	8.3169(3)	20.4484(7)	22.6673(8)	107.978(3)	99.002(3)	95.195(3)	3581.8(2)
170	8.2993(12)	20.451(5)	22.657(3)	107.873(18)	99.154(12)	95.553(16)	3569.7(12)
160	8.3156(14)	12.380(3)	17.649(3)	82.952(18)	78.826(15)	84.883(16)	1765.0(5)
150	8.3234(11)	12.374(3)	17.654(3)	82.840(18)	78.714(14)	85.075(14)	1765.6(6)
140	8.3273(15)	12.370(3)	17.608(3)	82.83(2)	78.660(17)	85.054(18)	1760.9(6)
125	8.3129(13)	12.3827(18)	17.511(6)	82.844(18)	78.463(19)	85.025(14)	1748.8(7)

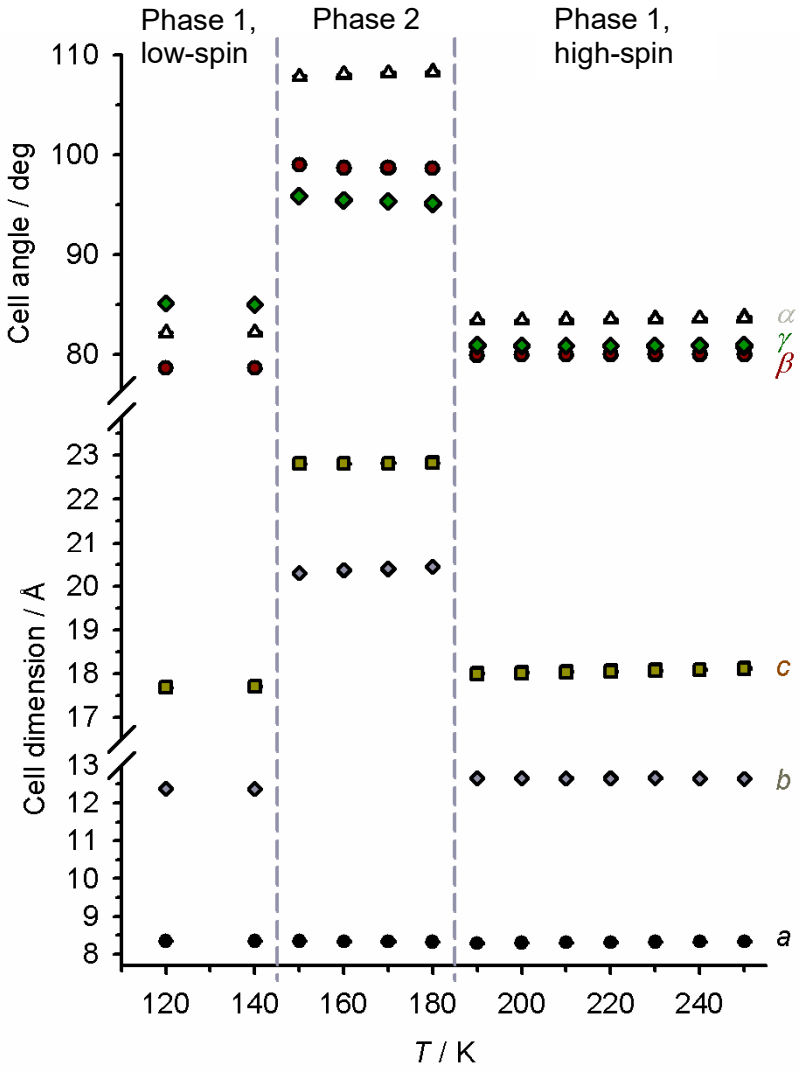

Figure S22 Variable temperature unit cell data for **1[ClO$_4$]$_2$**·EtCN (Table S9). Data were collected in cooling and warming temperature ramps, but no thermal hysteresis in the crystallographic phase changes is resolved.

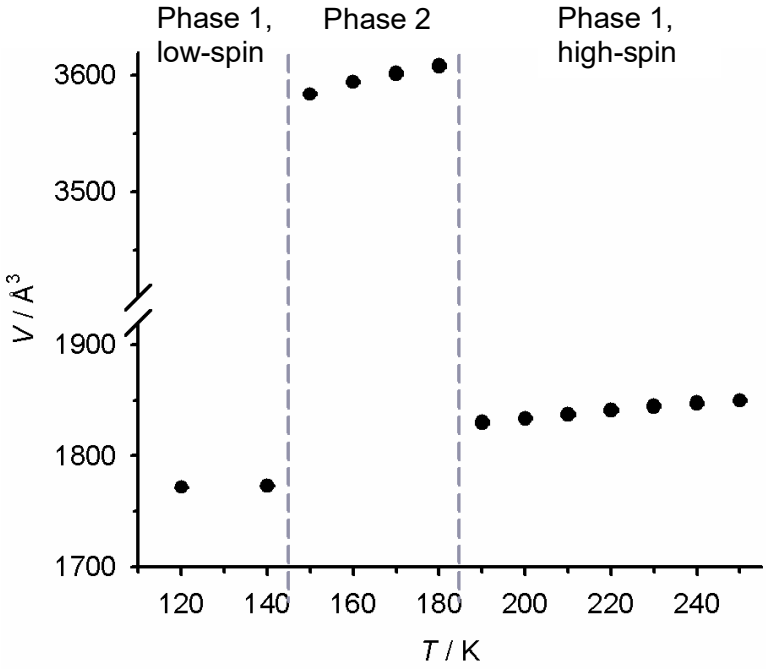

Figure S23 Variable temperature unit cell volumes for **1[ClO$_4$]$_2$**·EtCN. Details as for Figure S22.

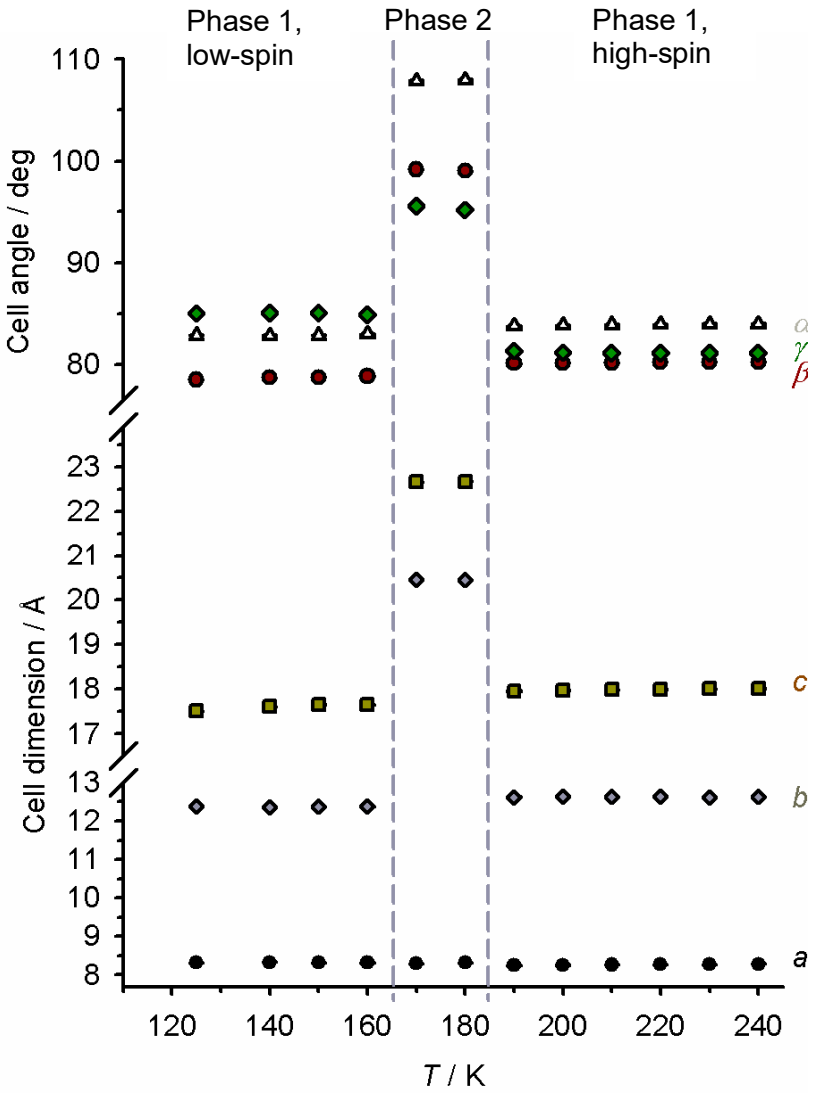

Figure S24 Variable temperature unit cell data for $\mathbf{1[BF_4]_{0.9}[ClO_4]_{1.1}}$·EtCN (Table S10). Data were collected in cooling and warming temperature ramps. Data were collected in cooling and warming temperature ramps, but no thermal hysteresis in the crystallographic phase changes is resolved.

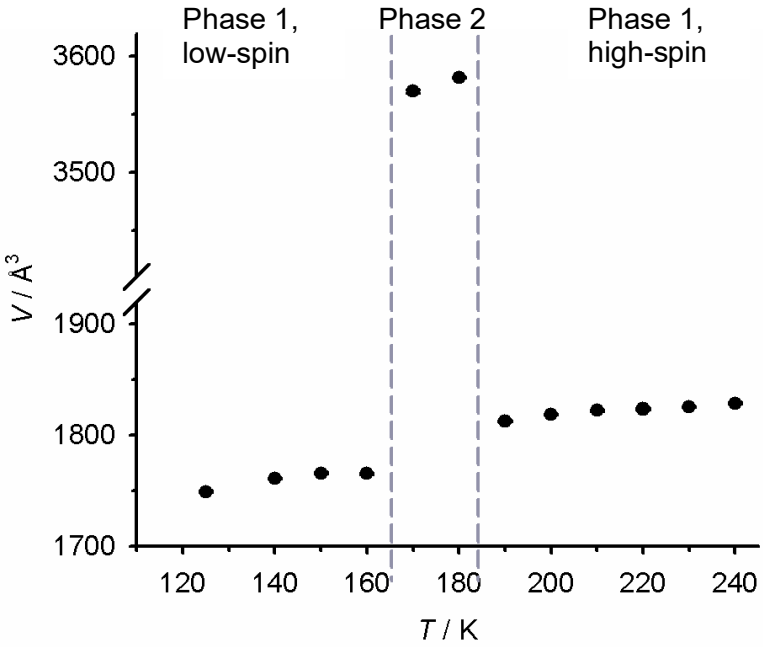

Figure S25 Variable temperature unit cell volumes for $\mathbf{1[BF_4]_{0.9}[ClO_4]_{1.1}}$·EtCN. Details as for Figure S24.

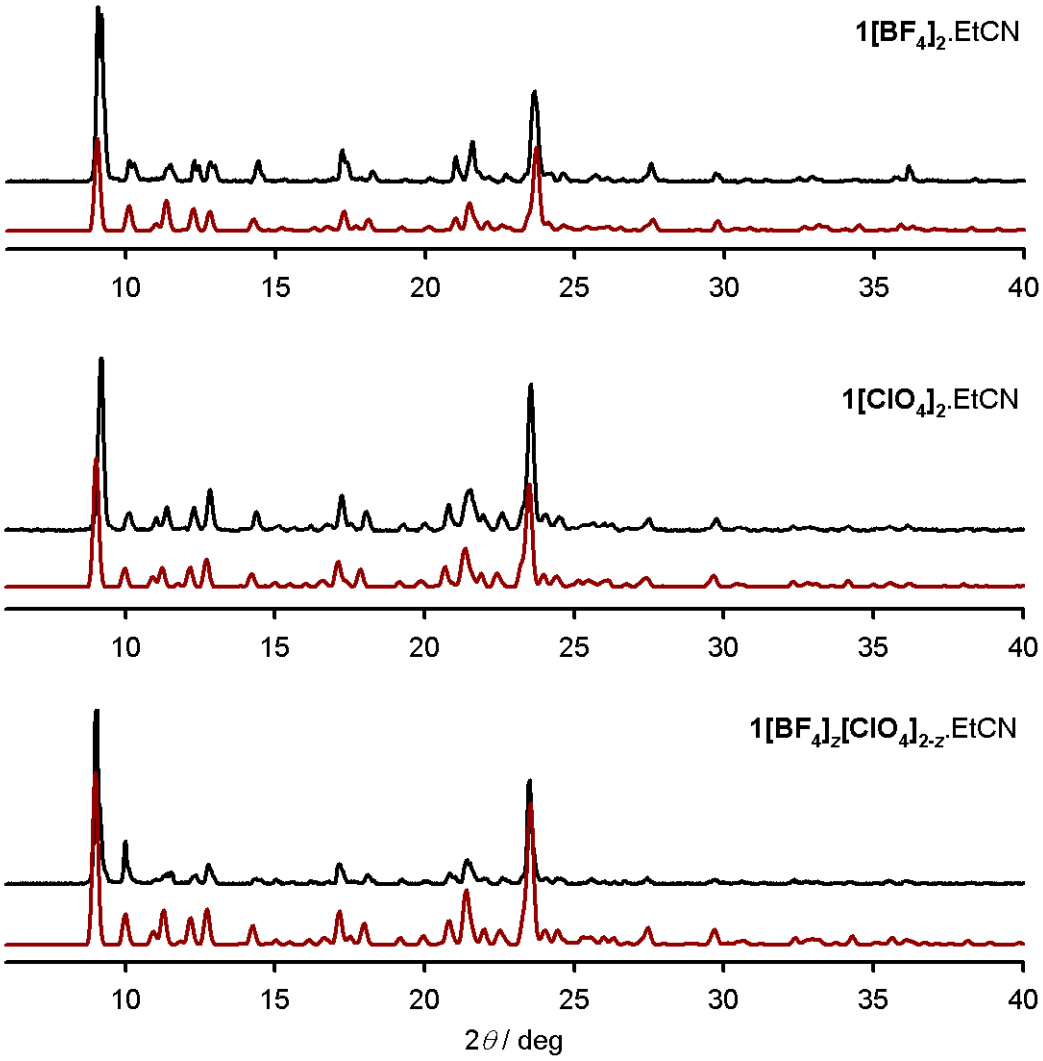

Figure S25 Measured (black) and simulated (red) room temperature X-ray powder diffraction data for the EtCN solvate materials.

All three powder patterns show excellent agreement with their simulations, showing these materials are phase-pure.

While the peak positions should match well, some differences in the measured and simulated peak intensities are to be expected in measurements of this type, which were performed on polycrystalline materials rather than ideal powders.

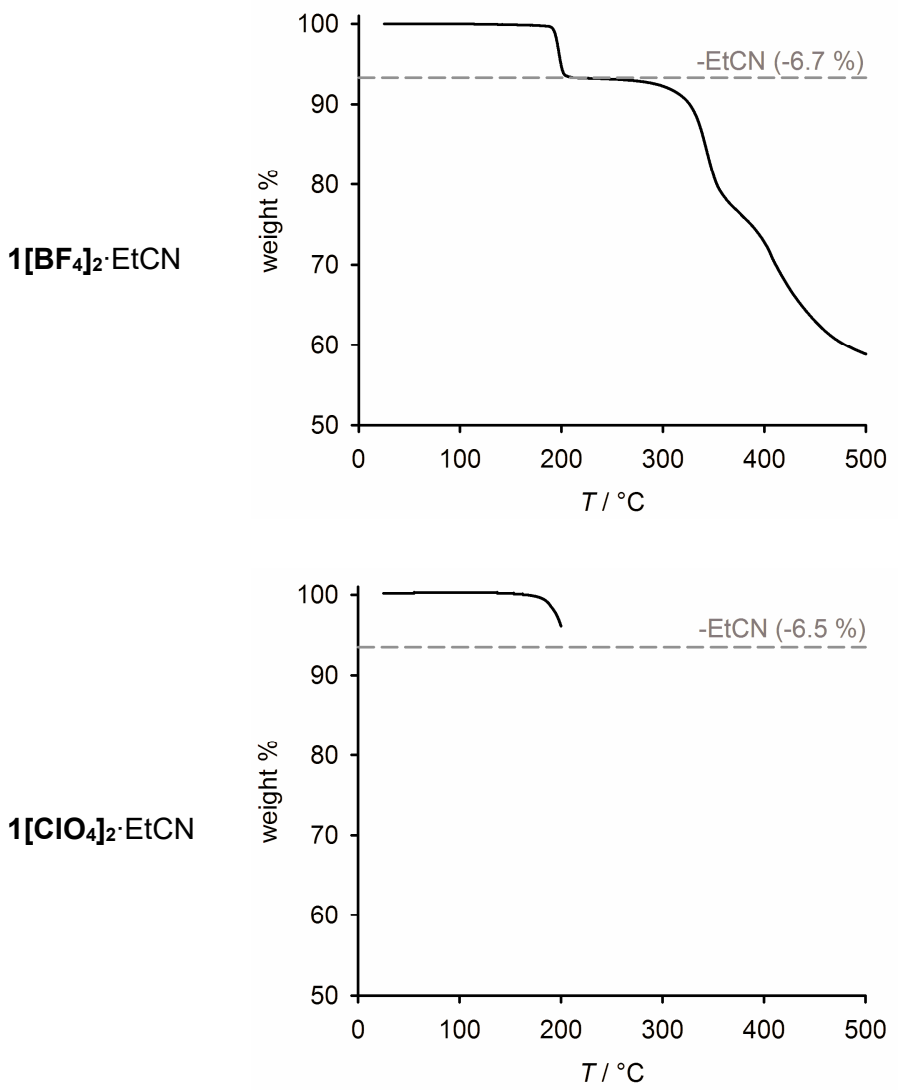

Figure S27 TGA data for **1[BF$_4$]$_2$**·EtCN and **1[ClO]$_2$**·EtCN. The perchlorate salt was not heated above 200 °C because of its risk of detonation.

The lattice solvent in **1[BF$_4$]$_2$**·EtCN is lost abruptly between 190-210 °C, with no significant mass loss occurring at lower temperatures. The perchlorate salt evidently behaves similarly, although its solvent loss is incomplete at 200 °C.

The high thermal stability of the**se** phases explains their stability to solvent loss inside the vacuum of the SQUID magnetometer cavity.

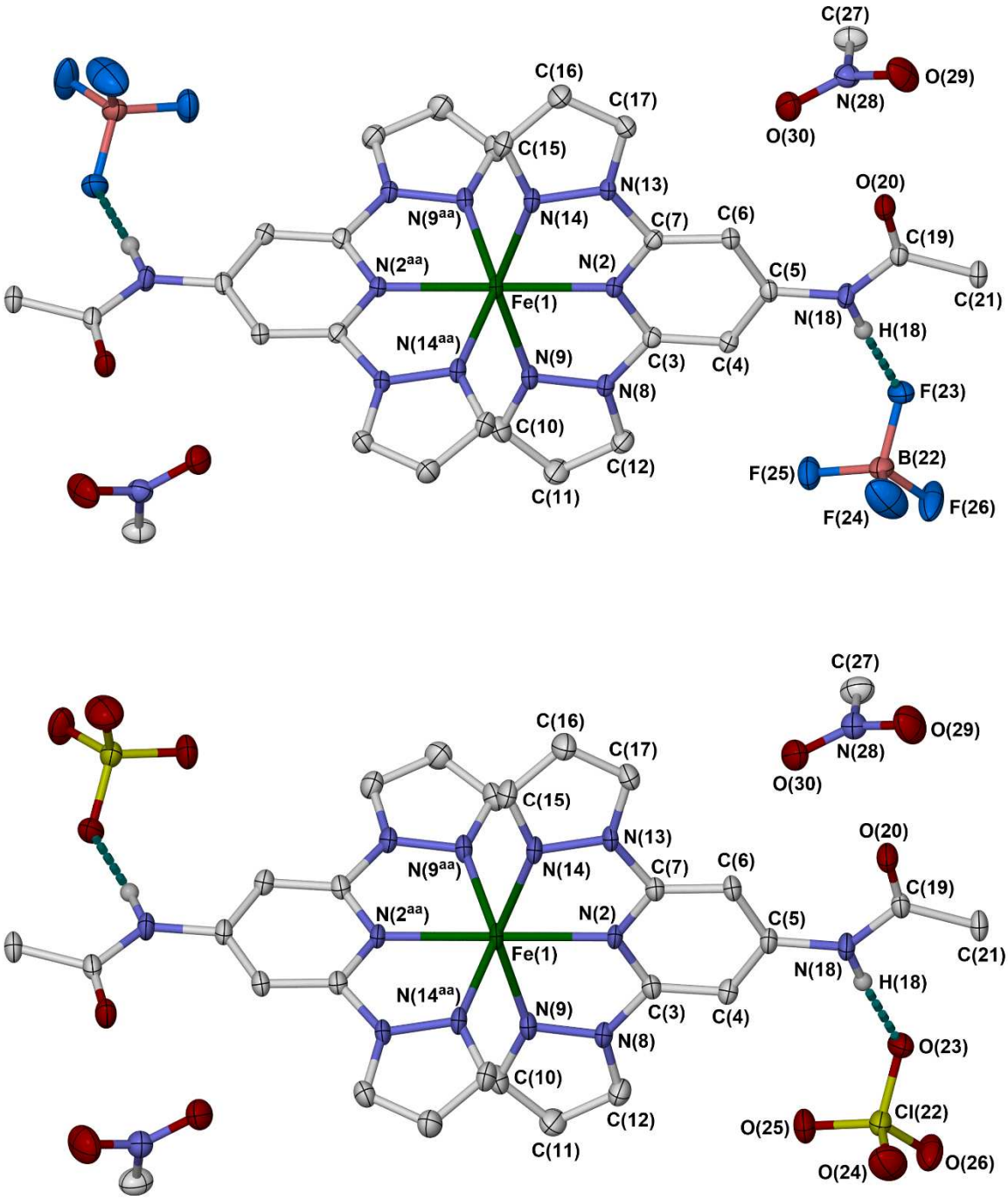

Figure S28 The asymmetric units of isomorphous **1[BF$_4$]$_2$**·2MeNO$_2$ (top) and **1[ClO$_4$]$_2$**·2MeNO$_2$ (bottom), with the full atom numbering scheme. Displacement ellipsoids are at the 50 % probability level, and C-bound H atoms are omitted for clarity. Symmetry code: (aa) 1−*x*, *y*, ½−*z*.

Colour code: C, white; H, pale grey; B, pink; Cl, yellow; F, cyan; Fe, green; N, blue; O, red.

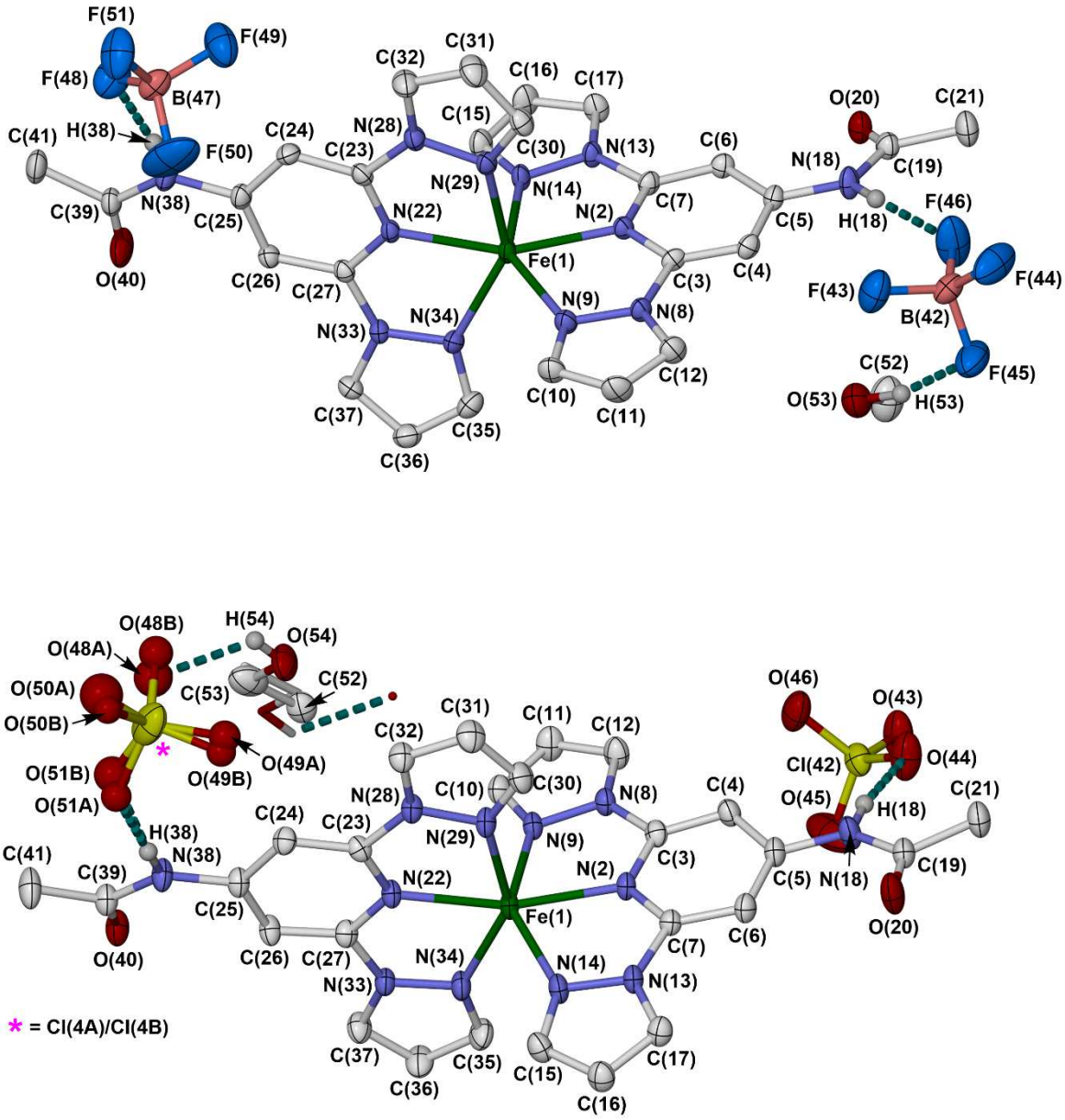

Figure S29 The asymmetric units of **1[BF$_4$]$_2$**·MeOH (top) and **1[ClO$_4$]$_2$**·½EtOH (bottom), with the full atom numbering scheme. Displacement ellipsoids are at the 50 % probability level, and C-bound H atoms are omitted for clarity.

Colour code: C, white; H, pale grey; B, pink; Cl, yellow; F, cyan; Fe, green; N, blue; O, red.

The ethanol molecule in [Fe*L*][ClO$_4$]$_2$·½EtOH is disordered about a crystallographic inversion centre. Its symmetry-related congener is also shown in the Figure, with de-emphasised atoms for clarity.

The disorder in the neighbouring anion Cl(47)-O(51) correlates with the orientation of the solvent molecule, adopting the 'A' site when the solvent is oriented towards it for hydrogen bonding and the 'B' site when the solvent hydroxyl group is oriented away from it.

Table S11 Selected bond lengths, angles and other structural parameters (Å , °, Å^3) for the other high-spin solvates of **1X$_2$** (X^- = BF_4^- or ClO_4^-). See Figures S28 and S29 for the atom numbering scheme, while definitions of V_{Oh}, Σ, Θ, φ and θ are given on page S10. Symmetry code: (aa) 1−*x*, *y*, ½−*z*.

	1[BF$_4$]$_2$·2MeNO$_2$[a]	**1[ClO$_4$]$_2$**·2MeNO$_2$[a]		**1[BF$_4$]$_2$**·MeOH	**1[ClO$_4$]$_2$**·½EtOH
T / K	120	120		120	120
Fe(1)–N(2)	2.1165(15)	2.1247(18)	Fe(1)–N(2)	2.141(3)	2.127(2)
Fe(1)–N(9)	2.2061(16)	2.206(2)	Fe(1)–N(9)	2.195(3)	2.199(2)
Fe(1)–N(14)	2.1776(16)	2.177(2)	Fe(1)–N(14)	2.211(3)	2.193(2)
			Fe(1)–N(22)	2.131(3)	2.135(2)
			Fe(1)–N(29)	2.220(3)	2.208(2)
			Fe(1)–N(34)	2.200(3)	2.197(2)
N(2)–Fe(1)–N(9)	73.44(5)	73.16(7)	N(2)–Fe(1)–N(9)	73.09(10)	73.25(8)
N(2)–Fe(1)–N(14)	73.54(5)	73.57(7)	N(2)–Fe(1)–N(14)	72.32(10)	72.86(9)
N(2)–Fe(1)–N(2^{i})	176.47(8)	175.29(11)	N(2)–Fe(1)–N(22)	158.32(11)	164.47(9)
N(2)–Fe(1)–N(9^{i})	104.22(5)	103.70(7)	N(2)–Fe(1)–N(29)	95.03(10)	94.03(9)
N(2)–Fe(1)–N(14$^{'}$)	108.85(5)	109.61(7)	N(2)–Fe(1)–N(34)	121.57(11)	120.39(9)
N(9)–Fe(1)–N(14)	146.93(5)	146.69(6)	N(9)–Fe(1)–N(14)	144.71(10)	144.51(8)
			N(9)–Fe(1)–N(22)	124.06(10)	99.82(8)
N(9)–Fe(1)–N(9^{i})	100.45(8)	99.85(11)	N(9)–Fe(1)–N(29)	92.37(11)	96.85(9)
N(9)–Fe(1)–N(14^{i})	89.27(6)	89.55(7)	N(9)–Fe(1)–N(34)	96.94(11)	91.93(9)
			N(14)–Fe(1)–N(22)	91.19(10)	115.60(9)
			N(14)–Fe(1)–N(29)	97.36(11)	95.71(9)
N(14)–Fe(1)–N(14^{i})	99.68(8)	99.98(11)	N(14)–Fe(1)–N(34)	95.16(11)	96.18(9)
			N(22)–Fe(1)–N(29)	72.71(10)	72.69(8)
			N(22)–Fe(1)–N(34)	72.76(10)	72.98(8)
			N(29)–Fe(1)–N(34)	143.38(10)	145.54(8)
V_{Oh}	12.385(7)	12.412(9)	V_{Oh}	12.119(10)	12.280(9)
Σ	153.8(2)	153.9(3)	Σ	162.8(4)	158.7(3)
Θ	495	499	Θ	548	529
ϕ	176.47(8)	175.29(11)	ϕ	158.32(11)	164.47(9)
θ	79.88(1)	79.55(1)	θ	86.39(3)	89.62(3)

[a]The asymmetric unit of this structure contains half a molecule, with Fe(1) lying on a crystallographic C_2 axis.

Table S12 Hydrogen bond parameters (Å , °) for the other high-spin solvates of **1X₂** (X^- = BF_4^- or ClO_4^-). See Figures S28 and S29 for the atom numbering scheme.

	N−H	H···X	N···X	N−H···X
1[BF_4]₂·2$MeNO_2$				
N(18)−H(18)···F(23)	0.88	1.94	2.8127(19)	170.6
1[ClO_4]₂·2$MeNO_2$				
N(18)−H(18)···O(23)	0.88	1.98	2.848(3)	169.8
1[BF_4]₂·MeOH				
N(18)−H(18)···F(46)	0.88	2.02	2.882(4)	167.3
N(38)−H(38)···F(48)	0.88	2.14	3.010(4)	169.5
O(53)−H(53)···F(45)	1.00(4)	1.85(4)	2.829(4)	165(4)
1[ClO_4]₂·½EtOH				
N(18)−H(18)···O(44)	0.88	2.22	3.080(4)	166.8
N(38)−H(38)···O(51A)/O(51B)	0.88	2.07/2.08	2.948(5)/2.939(6)	179.4/166.1
O(54)−H(54)···O(48A)	0.84	2.21	2.848(8)	132.5

.

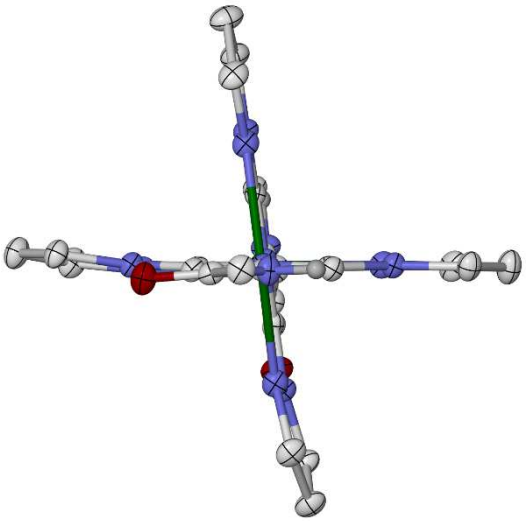

1[BF$_4$]$_2$·2MeNO$_2$
ϕ = 176.47(8)°
Θ = 79.88(1)°

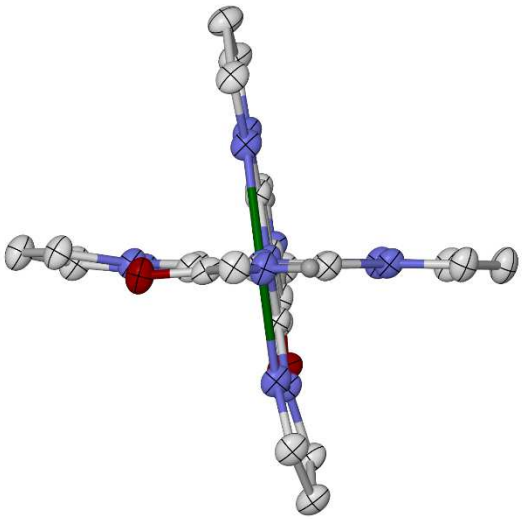

1[ClO$_4$]$_2$·2MeNO$_2$
ϕ = 175.29(11)°
Θ = 79.55(1)°

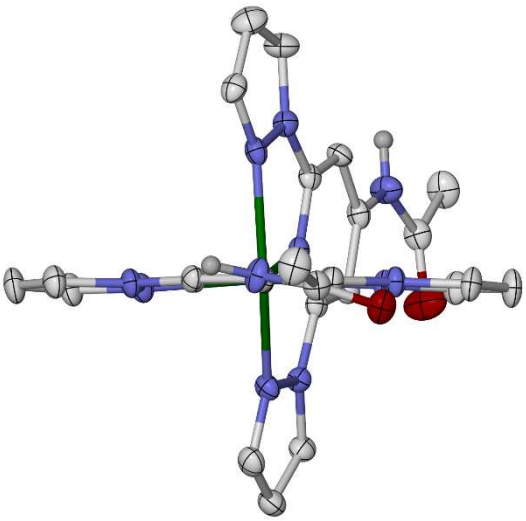

1[BF$_4$]$_2$·MeOH
ϕ = 158.32(11)°
Θ = 86.39(3)°

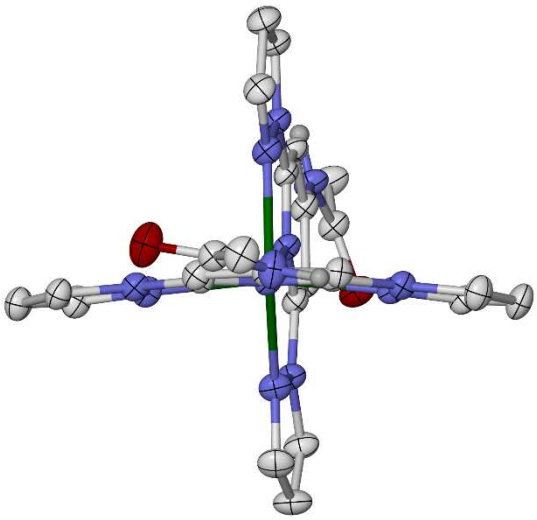

1[ClO$_4$]$_2$·½EtOH
ϕ = 164.47(9)°
Θ = 89.62(3)°

Figure S30 Alternative views of the high-spin cations in the nitromethane and alcohol solvates of **1[BF$_4$]$_2$** and **1[ClO$_4$]$_2$**, emphasising the distorted coordination geometries that probably inhibit them from undergoing spin-crossover on cooling. Each view is down one Fe−N{pyridyl} bond.

Colour code: C, white; H, pale grey; Fe, green; N, blue; O, red.

See page S10 for definitions of the ϕ and Θ parameters.

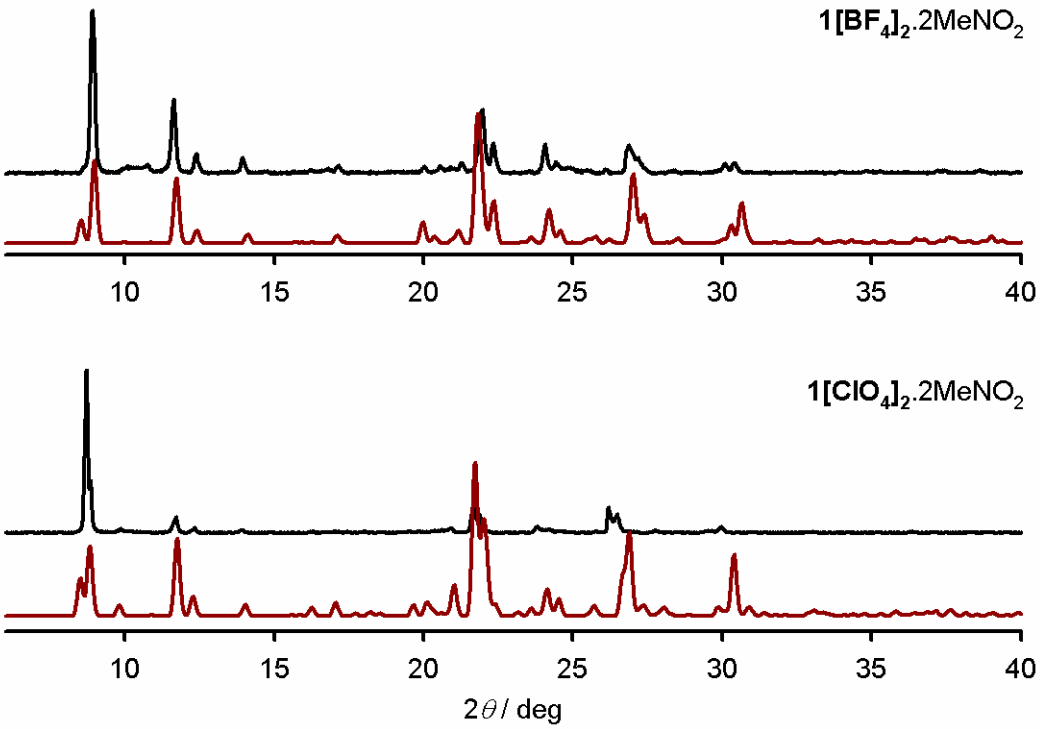

Figure S31 Measured (black) and simulated (red) room temperature X-ray powder diffraction data for the $MeNO_2$ solvate materials.

The general form of the measurements agrees with the simulated data, but some peak positions in both salts deviate from their simulation. This may reflect structural changes arising from partial solvent loss from the materials, before or during the measurement. Partial solvent loss from **1[ClO4]2**·2$MeNO_2$ is evident in its microanalysis, which is more consistent with a formulation of **1[ClO4]2**·$MeNO_2$ (page S3).

While the peak positions should match well, some differences in the measured and simulated peak intensities are to be expected in measurements of this type, which were performed on polycrystalline materials rather than ideal powders.

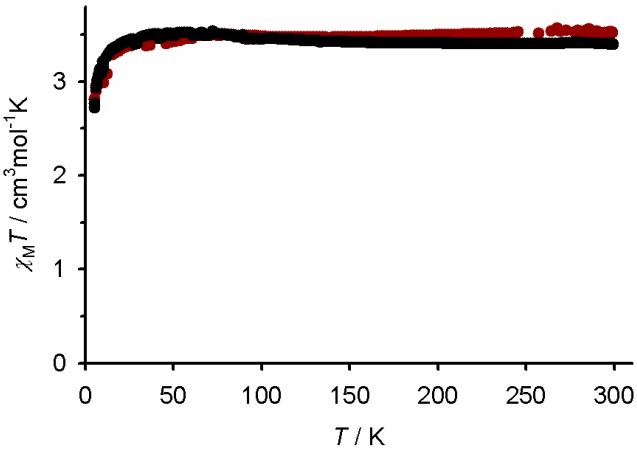

Figure S32 Variable temperature magnetic susceptibility data for **1[BF4]2**·2$MeNO_2$ (●) and **1[ClO4]2**·2$MeNO_2$ (●).

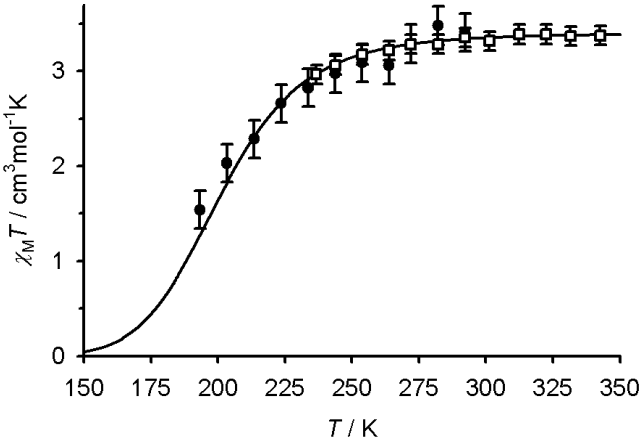

Figure S33 Variable temperature magnetic susceptibility data for **1[BF$_4$]$_2$** in $(CD_3)_2CO$ (●) and CD_3CN (○) solution.

The line shows the best fit of the data to eq 1 and 2.

$$\ln[(1 - n_{HS}(T))/\, n_{HS}(T)] = \Delta H/RT - \Delta S/R \quad (1)$$

$$\Delta S = \Delta H/T_{½} \quad (2)$$

The fitted parameters for the SCO equilibrium are $T_{½}$ = 201±2 K, ΔH = −21.5 kJ mol^{-1} and ΔS = 107 J mol^{-1} K^{-1}. The thermodynamic parameters are typical for a complex of this type.[17]

The data in $(CD_3)_2CO$ are noisier and have larger error bars, because the complex is less soluble in that solvent.

References

1. I. Capel Berdiell, R. Kulmaczewski, O. Cespedes and M. A. Halcrow, *Chem. Eur. J.*, 2018, **24**, 5055.
2. G. M. Sheldrick, *Acta Cryst. Sect. C.: Struct. Chem.*, 2015, **71**, 3.
3. L. J. Barbour, *J. Supramol. Chem.*, 2001, **1**, 189.
4. O. V. Dolomanov, L. J. Bourhis, R. J. Gildea, J. A. K. Howard and H. Puschmann, *J. Appl. Cryst.*, 2009, **42**, 339.
5. C. J. O'Connor, *Prog. Inorg. Chem.*, 1982, **29**, 203.
6. D. F. Evans, *J. Chem. Soc.*, 1959, 2003; E. M. Schubert, *J. Chem. Educ.*, 1992, **69**, 62.
7. B. García and J. C. Ortega, *J. Chem. Eng. Data***,** 1988, **33**, 200.
8. P. Guionneau, M. Marchivie, G. Bravic, J.-F. Létard and D. Chasseau, *Top. Curr. Chem.*, 2004, **234**, 97.
9. I. Capel Berdiell, R. Kulmaczewski and M. A. Halcrow, *Inorg. Chem.*, 2017, **56**, 8817.
10. J. K. McCusker, A. L. Rheingold and D. N. Hendrickson, *Inorg. Chem.*, 1996, **35**, 2100.
11. M. A. Halcrow, *Coord. Chem. Rev.*, 2009, 253, 2493.
12. L. J. Kershaw Cook, R. Mohammed, G. Sherborne, T.D. Roberts, S. Alvarez and M. A. Halcrow, *Coord. Chem. Rev.*, 2015, **289–290**, 2.
13. J. M. Holland, J. A. McAllister, C. A. Kilner, M. Thornton-Pett, A. J. Bridgeman and M. A. Halcrow, *J. Chem. Soc., Dalton Trans.*, 2002, 548.
14. S. Vela, J. J. Novoa and J. Ribas-Arino, *Phys. Chem. Chem. Phys.*, 2014, **16**, 27012.
15. For other examples of high-spin $[Fe(bpp)_2]^{2+}$ derivatives with distorted coordination geometries see ref. 17, and the following references:

    J. Elhaïk, D. J. Evans, C. A. Kilner and M. A. Halcrow, *Dalton Trans.*, 2005, 1693;

    J. Elhaïk, C. A. Kilner and M. A. Halcrow, *Dalton Trans.*, 2006, 823;

    C. A. Kilner and M. A. Halcrow, *Polyhedron*, 2006, **25**, 235**;**

    M. Haryono, F. W. Heinemann, K. Petukhov, K. Gieb, P. Müller and A. Grohmann, *Eur. J. Inorg. Chem.*, 2009, 2136;

    R. González-Prieto, B. Fleury, F. Schramm, G. Zoppellaro, R. Chandrasekar, O. Fuhr, S. Lebedkin, M. Kappes and M. Ruben, *Dalton Trans.*, 2011, **40**, 7564;

    Y. Hasegawa, R. Sakamoto, K. Takahashi and H. Nishihara, *Inorg. Chem.*, 2013, **52**, 1658;

    L. Pukenas, F. Benn, E. Lovell, A. Santoro, L. J. Kershaw Cook, M. A. Halcrow and S. D. Evans, *J. Mater. Chem. C,* 2015, **3**, 7890;

    N. Bridonneau, L. Rigamonti, G. Poneti, D. Pinkowicz, A. Forni and A. Cornia, *Dalton Trans.*, 2017, **46**, 4075;

    I. Šalitroš, R. Herchel, O. Fuhr, R. González-Prieto and M. Ruben, *Inorg. Chem.*, 2019, **58**, 4310;

    I. Capel Berdiell, R. Kulmaczewski, S. L. Warriner, O. Cespedes and M. A. Halcrow, *Eur. J. Inorg. Chem.*, 2020, 4334.
16. L. J. Kershaw Cook, F. L. Thorp-Greenwood, T. P. Comyn, O. Cespedes, G. Chastanet and M. A. Halcrow, *Inorg. Chem.*, 2015, **54**, 6319;

    K. S. Kumar, B. Heinrich, S. Vela, E. Moreno-Pineda, C. Bailly and M. Ruben, *Dalton Trans.*, 2019, **48**, 3825.
17. L. J. Kershaw Cook, R. Kulmaczewski, R. Mohammed, S. Dudley, S. A. Barrett, M. A. Little, R. J. Deeth and M. A. Halcrow, *Angew. Chem. Int. Ed.*, 2016, **55**, 4327.